

Review

Cathodes for Zinc-Ion Micro-Batteries: Challenges, Strategies, and Perspectives

Ling Deng ^{1,2}, Qunfang Lin ¹, Zeyang Li ¹, Juexian Cao ^{1,*}, Kailing Sun ^{1,*} and Tongye Wei ¹ 

¹ School of Physics and Optoelectronics & Hunan Institute of Advanced Sensing and Information Technology, Xiangtan University, Xiangtan 411105, China; 202131520134@smail.xtu.edu.cn (L.D.); 20232152133@smail.xtu.edu.cn (Q.L.); 202331520172@smail.xtu.edu.cn (Z.L.); weity@xtu.edu.cn (T.W.)

² School of Energy, Mechanical and Electrical Engineering, Hunan University of Humanities, Science and Technology, Loudi 417000, China

* Correspondence: jxcao@xtu.edu.cn (J.C.); skl2020@xtu.edu.cn (K.S.)

Abstract: The sustainable development of high-performance micro-batteries, characterized by miniaturized size, portability, enhanced safety, and cost-effectiveness, is crucial for the advancement of wearable and smart electronics. Zinc-ion micro-batteries (ZIMBs) have attracted widespread attention for their high energy density, environmental friendliness, excellent safety, and low cost. The key to designing high-performance ZIMBs lies in improving their volumetric capacity and cycle stability. This review focuses on material design, electrode fabrication, and the structural configuration of micro-batteries, providing a comprehensive analysis of the challenges and strategies associated with cathodes in ZIMBs. Additionally, the application of ZIMBs, which provide energy for electronics such as wearable devices, tiny robots, and sensors, is introduced. Finally, future perspectives on cathodes for ZIMBs are discussed, offering key insights into their design and fabrication in order to facilitate the successful integration of ZIMBs into practical applications.

Keywords: zinc-ion micro-batteries; cathode materials; microelectrode fabrication; structural configurations



Academic Editor: Marco Giorgetti

Received: 27 December 2024

Revised: 26 January 2025

Accepted: 27 January 2025

Published: 2 February 2025

Citation: Deng, L.; Lin, Q.; Li, Z.; Cao, J.; Sun, K.; Wei, T. Cathodes for Zinc-Ion Micro-Batteries: Challenges, Strategies, and Perspectives. *Batteries* **2025**, *11*, 57. <https://doi.org/10.3390/batteries11020057>

Copyright: © 2025 by the authors. Licensee MDPI, Basel, Switzerland. This article is an open access article distributed under the terms and conditions of the Creative Commons Attribution (CC BY) license (<https://creativecommons.org/licenses/by/4.0/>).

1. Introduction

In recent years, the swift advancement of the IoT has stimulated the booming growth of smart and wearable microelectronics, tiny robots, implantable medical devices, wireless self-powered systems, and more applications. In this context, miniature energy storage devices, characterized by miniaturized size, portability, enhanced safety, and cost-effectiveness, have become vital for powering microelectronic products [1–4]. Among various micro-batteries, zinc-ion micro-batteries (ZIMBs) have attracted widespread attention for their high energy density, environmental friendliness, excellent safety, and low cost. These merits make ZIMBs highly promising candidates for powering next-generation devices, such as wearable electronics, tiny robots, and portable medical devices.

Zn's high theoretical volumetric energy density (5855 mAh cm⁻³) and low electrochemical potential (−0.76 V vs. SHE) enable its operation in aqueous electrolytes, further reducing costs and minimizing fire risks. In addition, ZIBs with aqueous electrolytes exhibit much higher ionic conductivity (10⁻¹–1 S cm⁻¹) compared to non-aqueous electrolytes (1–10 mS cm⁻¹), further enabling fast-rate capacity [3,5]. However, significant challenges remain in the development of ZIMBs, particularly regarding their cathodes. The cathode is crucial in determining the capacity, rate capability, and cycle life, factors which largely

influence the overall performance of ZIMBs. Therefore, understanding and addressing the limitations of the cathode is essential for advancing ZIMB technology.

Generally, micro-batteries (MBs) have a small footprint, typically in the range of square millimeters or square centimeters, with electrode thickness restricted to the micron level or to sub-cubic-millimeter volumes for 3D configurations [6,7]. It is noted that, unlike conventional batteries, achieving high electrochemical performance is more challenging for MBs due to their limited space or footprint area. The electrode serves as the key component of MBs, with its material composition, microstructure, fabrication techniques and spatial configuration collectively influencing the overall electrochemical performance of MBs. Hence, the design of both electrode materials and architectures requires ingenuity and modern fabrication techniques in order to achieve high-performance MBs.

Recently, significant efforts have been focused on regulating the microstructures of electrode materials through engineering techniques such as crystal structure selection, morphology design, defect engineering, and interlayer engineering [8–11]. Additionally, combining electrode materials with highly conductive nanoporous frameworks to achieve both high energy storage and rapid power delivery has also been a key focus [12,13]. From an architectural perspective, the distinctive design of the electrode minimizes ion transfer pathways, enhancing both rate capability and power density. Furthermore, these MBs are well suited to the shape customizability and aesthetic versatility of microelectronics. For example, 3D MBs have been employed to simultaneously enhance high energy density and power capability. These 3D electrode architectures offer high surface-to-volume ratios, optimizing mass loading and minimizing ion diffusion pathways [14]. The development of electrode architectures benefits from advances in fabrication techniques, such as photolithography, screen printing, laser scribing, electrodeposition, and direct ink writing (DIW). Finally, these feasible electrodes are assembled into devices for diverse applications [15–17].

In this review, we concentrate on cathode material design, electrode fabrication, and the structural configurations of MBs, providing a comprehensive analysis of the challenges and strategies associated with cathodes in ZIMBs. Additionally, the applications of ZIMBs, which power electronics such as wearable devices, flexible robots, and sensors, are introduced. Finally, future perspectives on cathodes for ZIMBs are discussed, offering key insights into their design and fabrication to facilitate the successful integration of ZIMBs into practical applications.

2. Challenges and Optimization Strategies for Cathode Materials

ZIBs are primarily composed of the cathode, anode, and electrolyte. In some cases, they include current collectors and separators. The cathode plays a critical role in determining the electrochemical performance of ZIBs. Cathode materials for large-scale energy storage are required to possess an optimal reversible charge-discharge capacity, outstanding cycle stability, abundant resources, and environmental friendliness [9]. Therefore, developing a comprehensive understanding of the challenges and corresponding optimization strategies for the current cathode materials is essential before rational utilization.

2.1. Challenges of Cathode Materials

Numerous studies have been conducted on cathode materials for ZIBs. However, persistent challenges remain, including poor structural stability, the dissolution of active materials, low electrical conductivity, and side reactions, all of which significantly hinder their practical application and development.

2.1.1. Poor Structural Stability

Because of its large size (0.76 Å) and strong electrostatic attraction, the Zn²⁺ ion readily forms tight bonds with electronegative atoms (such as oxygen), inducing substantial stress in host during insertion/extraction, which can cause phase transformation or structural collapse eventually. As shown in Figure 1a, due to the insertion of hydrated Zn²⁺, tunnel-structured MnO₂ transitions to display a layered structure. Subsequently, the structure collapses owing to the repeated intercalation of hydrated Zn²⁺, leading to a rapid decline in capacity during cycling [18]. This issue is common in V-based and Mn-based cathode materials with multiple polymorphic forms. Zn²⁺ intercalation weakens the V-O bond, creating a rivalrous interaction between V-O and Zn-O bond. This leads to a prominent reduction in the thermodynamic stability. With ongoing intercalation/extraction, the lattice spacing suffers persistent expansion and contraction, ultimately causing structural collapse. The stress and spatial deformation produced during phase transitions aggravate lattice distortion, decrease Zn²⁺ ion active sites, and prevent migration [9]. Layered structures, typically bonded by weaker van der Waals forces, experience more significant structural collapse. It is crucial to modify and optimize cathode materials to fulfill application demands.

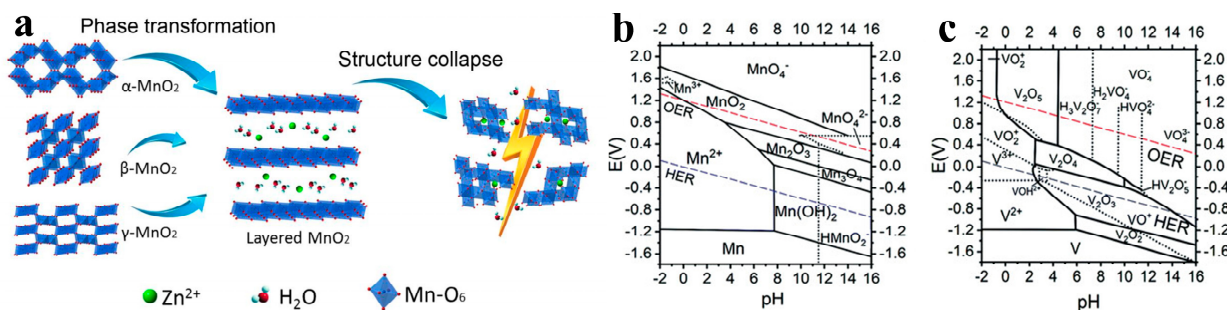


Figure 1. (a) Structural transformation of MnO₂ during discharge/charge cycles. Reprinted with permission from ref. [18]. Copyright 2018, Springer Nature. (b) Pourbaix diagram for (b) manganese and (c) vanadium, oxides. Reprinted with permission from ref. [19]. Copyright 2023, John Wiley and Sons.

2.1.2. Dissolution of Cathode Materials

In aqueous ZIBs, the electrochemical reaction of cathode materials varies according to the pH of the electrolyte. Weakly acidic aqueous electrolytes are preferred due to their low corrosiveness and excellent compatibility with the zinc anode. Nevertheless, these electrolytes may lead to the dissolution of cathode materials, a process that is further aggravated by the increased protons produced from water splitting. Consequently, the cathode materials experience structural degradation, leading to battery failure owing to insufficient cycling stability. Generally, Jahn-Teller effect has a significant influence on MnO_2 [19]. In weakly acidic aqueous electrolytes, Mn^{4+} reduces to Mn^{3+} during the discharge process. Mn^{3+} is prone to the Jahn-Teller distortion, and the disproportionation reaction results in the dissolution of Mn^{2+} . As shown in Figure 1b,c, both V-based and Mn-based materials tend to dissolve during cycling in aqueous ZIBs, particularly in the presence of mildly acidic electrolytes [10].

2.1.3. Poor Electrical Conductivity

Mn-based and V-based cathode materials exhibit semiconductor properties [20]. Generally, most electrons in semiconductors are confined within covalent bonds. However, a small number of electrons escape from these bonds due to thermal motion, becoming free electrons and leaving behind holes in the original covalent bonds. In this scenario, the holes carry a positive charge, and in the semiconductor, both free electrons and holes serve as charge carriers [9]. V-based and Mn-based materials exhibit poor electronic conductivity because of the limited availability of free electrons and holes. The inadequate intrinsic conductivity, which results in both limited ionic diffusion and sluggish reaction kinetics, can lead to significant electrochemical polarization, ultimately resulting in suboptimal capacity and poor rate performance.

2.1.4. Parasitic Byproducts Formation

The reduplicative charge and discharge process promotes the formation of unforeseen byproducts. Side reactions, such as oxygen evolution (OER) and hydrogen evolution (HER), are pH-dependent and thus under the influence of the concentration and composition of the electrolytes [21,22]. Numerous zinc salt byproducts are produced at the cathode electrode by repeated discharging/charging cycles, contributing to the increased interfacial impedance and capacity degradation of cathode materials.

For cathodes with H^+ intercalation, byproducts such as layered double hydroxides form due to the increased local OH^- concentration on the cathode due to H^+ consumption. The generated OH^- reacts with Zn^{2+} and anions in the aqueous electrolyte, and the byproduct species are determined by the type of anion. Generally speaking, $Zn_4SO_4(OH)_6 \cdot 5H_2O$ is the primary byproduct in a $ZnSO_4$ aqueous electrolyte, whereas $Zn_x(CF_3SO_3)_y(OH)_{2x-y} \cdot nH_2O/Zn_{12}(CF_3SO_3)_9(OH)_{15} \cdot xH_2O$ byproducts are commonly found when using a $Zn(CF_3SO_3)_2$ aqueous electrolyte. In addition to the pH influence, factors such as active water molecules, dissolved O_2 molecules, and Mn^{3+} ions are also identified as contributors to byproduct formation [23,24]. The generation of unexpected byproducts continues to be one of the most critical and challenging issues in aqueous ZIBs, ultimately resulting in poor cycling performances.

2.2. Strategies for Developing Advanced Cathodes

To address the aforementioned challenges, numerous studies have focused on constructing novel structures that offer substantial capacity while maintaining stability during Zn^{2+} insertion/extraction. Recent research efforts in material engineering have primarily concentrated on areas such as nanostructure design, improvements in electrical conductivity, interlayer engineering, and defect engineering.

2.2.1. Nanostructure Design

Generally, nanostructured materials with notable size effects and high surface areas are used in a common approach to enhancing energy storage. The benefits of those materials arise from the following advantages. (1) Nanostructure optimization increases the contact surface between the electrolyte and electrode, enhancing Zn^{2+} storage sites. The smooth diffusion of charge carriers on the nanostructure surface significantly enhances rate capability. (2) Nanostructures, such as 1D nanowires, nanorods, and nanobelts, shorten the ion diffusion path, therefore enhancing the reaction kinetics. (3) Nanostructures reduce volume expansion and maintain structural stability, contributing to stable cycling performances.

So far, various nanostructures, such as low-dimensional structures, hierarchical structures, and hollow structures, have been designed to optimize Zn^{2+} storage. As an illustration, Jing et al. [25] synthesized an amorphous $Mn_{1.8}Fe_{1.2}O_4$ material with a hollow

nanocube structure for ZIBs (Figure 2a,b). The amorphous characteristics facilitated diffusion and narrowed the band gap, leading to improved Zn^{2+} ion and electron transport kinetics. In addition, the hollow structure supplied ample sites and suppressed structural collapse during constant cycling. Liu et al. [26] developed hollow octahedral Pr_6O_{11} - Mn_2O_3 heterostructures (Figure 2c,d). Pr_6O_{11} not only effectively inhibited the Mn dissolution, stabilizing Mn_2O_3 , but also induced charge rearrangement at the interface, promoting ion/electron transfer and improving the electrochemical activity and stability of Pr_6O_{11} - Mn_2O_3 . The hollow structure designed offered sufficient sites and facilitated the reaction kinetics.

2.2.2. Improving Electrical Conductivity

Electrical conductivity is a crucial factor influencing reaction kinetics in ZIBs. Due to the inherently low electronic conductivity of certain materials (e.g., MnO_2 and V_2O_5), combining them with conductive materials such as carbon substances and conductive polymers has emerged as an effective strategy with which to enhance their electronic conductivity. Moreover, this approach has been shown to increase the surface area, provide more storage sites, and improve the stability of the microstructure.

Owing to their high conductivity, light weight, and outstanding mechanical flexibility, carbon materials such as carbon nanotubes (CNTs) and graphene are widely adopted in composites [12,13,27,28]. As shown in Figure 2e,f, a hydrogen-substituted graphdiyne (HsGDY) film was tightly constructed on MnO_2 nanorods (denoted as MnO_2 -NRs@HsGDY) through interfacial modification [29]. The introduction of HsGDY significantly enhanced the conductivity of MnO_2 -NRs@HsGDY, reducing the charge transfer impedance (R_{ct}) from $249\ \Omega$ to $3.46\ \Omega$. Moreover, the conductive film contributed additional ion storage sites and enhanced structural stability via the accumulation of Zn^{2+} ions and the restriction of Mn^{2+} ions on the MnO_2 -NR surface. A pomegranate-like V_2O_5 @LIG composite was developed by anchoring V_2O_5 nanospheres onto the laser-induced graphene (LIG) conductive network through defect-induced adsorption [30]. The 3D porous and continuous electron conduction network provides adequate chemical active sites and ion transport channels (Figure 2g,h). Notably, the honeycomb-like LIG improved the electrical conductivity of the cathode by up to four orders of magnitude.

In addition to carbon materials, conductive polymers (e.g., PPy, PEDOT, PANI) with outstanding conductivity and excellent chemical stability are also commonly used as additives to enhance electron conductivity. As shown in Figure 2i,j, MnO_2 @PANI core-shell nanowires were prepared [31]. A uniform 6 nm thick conductive PANI layer was adhered to the surface of the MnO_2 nanowires, substantially increasing their electronic conductivity. The R_{ct} of the MnO_2 @PANI electrode was $177\ \Omega$, approximately one-third of that of pure MnO_2 (Figure 2k). Furthermore, the hybrid electrode showed a significantly smaller slope (12.1) compared to pure MnO_2 (49.1) (Figure 2l), indicating a higher ion diffusion coefficient. Both the reduced resistance and enhanced ion diffusion were attributed to the PANI shell. Similarly, PEDOT was uniformly coated on MnO_2 microspheres (denoted as MOP-5) to stabilize the structure and improve conductivity through polymerization [32]. As shown in Figure 2m–o, a 4 nm thick PEDOT layer was observed on the surface MnO_2 . The R_{ct} of MOP-5 ($51\ \Omega$) was significantly lower than that of MnO_2 ($371\ \Omega$) (Figure 2p), demonstrating that the PEDOT coating effectively improved electrical conductivity.

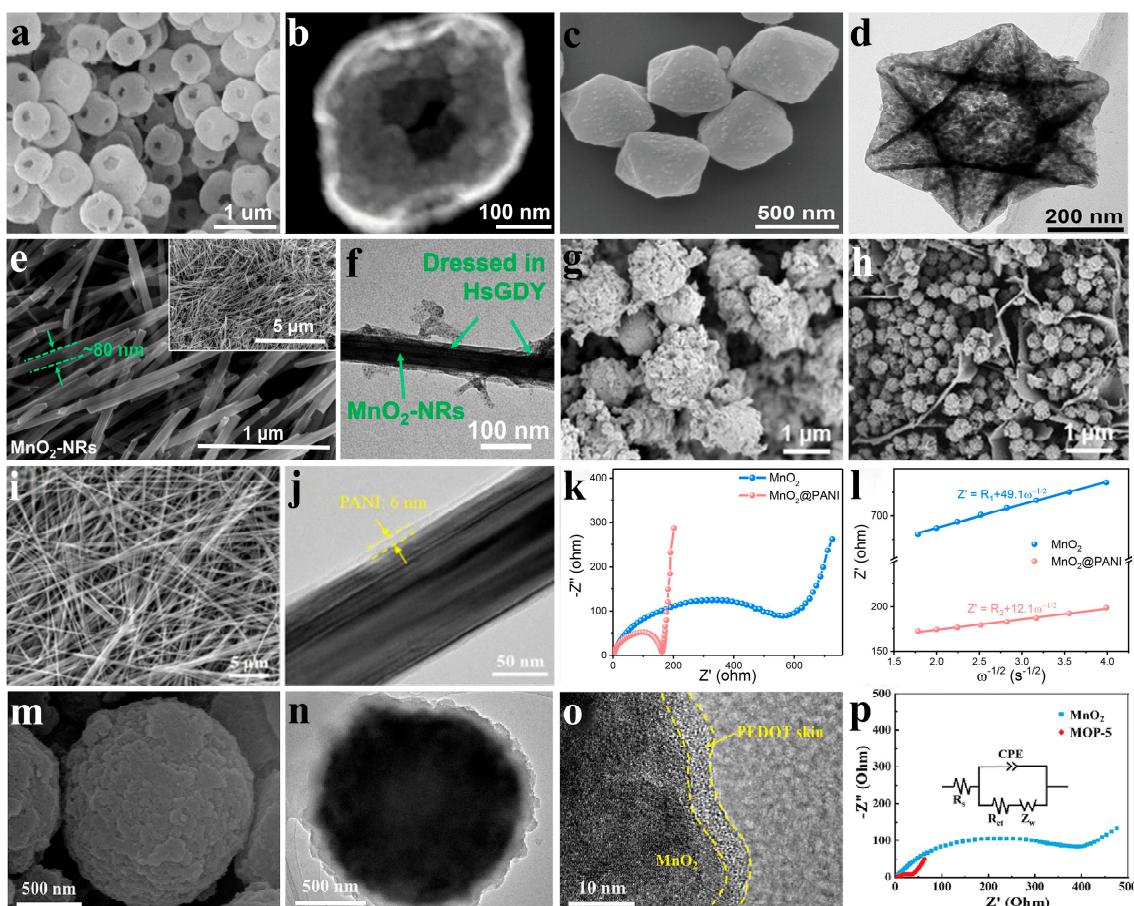


Figure 2. (a) SEM and (b) TEM images of a-H-MnFeO. Reprinted with permission from ref. [25]. Copyright 2023, Elsevier. (c) SEM and (d) TEM images of Pr/Mn-MIL-100. Reprinted with permission from ref. [26]. Copyright 2024, Wiley-VCH GmbH. (e) SEM and (f) TEM images of MnO₂-NRs@HsGDY. Reprinted with permission from ref. [29]. Copyright 2023, Elsevier. Morphology of V₂O₅@LIG with different composite amounts of LIG: (g) 0%, (h) 22%. Reprinted with permission from ref. [30]. Copyright 2024, Wiley-VCH GmbH. (i) SEM and (j) TEM images of MnO₂@PANI nanowires. (k) Nyquist plots of MnO₂@PANI and MnO₂ electrodes and (l) the corresponding linear plots of Z' vs. $\omega^{-1/2}$. Reprinted with permission from ref. [31]. Copyright 2023, Elsevier. (m) SEM, (n) TEM, and (o) HRTEM images of the MOP-5 microsphere. (p) Nyquist plots of MOP-5 and MnO₂ electrodes. Reprinted with permission from ref. [32]. Copyright 2023, Elsevier.

2.2.3. Interlayer Engineering

Because of the intercalation/deintercalation storage mechanism, hydrated Zn²⁺ ions are predominantly stored in tunnel-based or layered structures. For cathode materials with such structures, the narrowed interlayer spacing and unstable framework significantly hinder Zn²⁺ diffusion, making the structure susceptible to collapse during repeated Zn²⁺ intercalation and deintercalation cycles. Interlayer engineering effectively expands the interlayer spacing and stabilizes the host structure, ensuring Zn²⁺/H⁺ intercalation and deintercalation.

Various efforts have been conducted to insert guests into host layered lattices. For instance, the pre-intercalation of metal ions, such as K⁺, Na⁺, Cu²⁺, Mg²⁺, Ca²⁺, Al³⁺, and Bi³⁺, was explored to enhance the performance of MnO₂ [33–39]. Wang et al. [40] reported that Mg²⁺ doping in NH₄V₄O₁₀ acts as pillars, which expanding the interlayer spacing to 10.5 Å (from the original spacing of 9.6 Å). Meanwhile, pre-intercalated Mg²⁺ improves structural stability, resulting in an outstanding electrochemical performance.

Other intercalating guests, such as polymer molecules (PEDOT, PPY, PANI, PPY), have also been explored to adjust the interlayer spacing of active materials [41–44]. The intercalation of conductive polymer molecules and highly stable polymers can improve electrical conductivity and shield the intense electrostatic interaction between Zn^{2+} ion and the host materials, respectively. For example, our team developed a strategy of incorporating conductive polyaniline into V_2O_5 to enhance structural stability [43]. Analogically, Zhang et al. [45] synthesized Bet-intercalated MnO_2 (MnO_2 -Bet) by leveraging zwitterionic betaine (Bet) for intercalation. The quaternary ammonium groups in Bet, carrying positive charges, form strong electrostatic interactions with negatively charged oxygen atoms, bolstering structural stability and preventing collapse. Meanwhile, the carboxylate groups, with negative charges, promote efficient H^+ / Zn^{2+} diffusion, enhancing reaction kinetics.

2.2.4. Defect Engineering

Defect engineering has gradually become a strategic approach with which to adjust the electronic structures and lattice arrangement of cathode materials [46]. Ongoing studies mainly concentrate on point defects at the atomic scale, which include cation vacancies, anion vacancies, and doping. These defects adjust the local electronic structure and bring new electronic and electrochemical properties, such as enhanced conductivity and the creation of more sites.

As a common anion vacancy, oxygen vacancy (V_O) is widely used to modify the surface chemistry of cathode materials for ZIBs. Oxygen vacancies can adjust the local electronic structure. This affects the Gibbs free energy of Zn^{2+} adsorption on the surface, facilitating reversible Zn^{2+} intercalation/deintercalation. On the other hand, oxygen vacancies can reduce stress and electrostatic repulsion between nearby layers, which helps to overcome transfer and diffusion obstacles, enhancing charge transfer and ion diffusion during the reversible Zn^{2+} intercalation/deintercalation [9]. Under low oxygen pressure or reduction conditions, oxygen atoms are easily extracted from the lattice, creating oxygen vacancies. For instance, oxygen vacancies were introduced into α - MnO_2 by treating it with $NaBH_4$, which weakened the $Zn-O$ bond and facilitated the involvement of more electrons during charge/discharge [47]. Studies have shown that oxygen defects can improve conductivity by altering the local electronic structure. Combining defect engineering with other modification approaches, such as nanostructure design and interlayer engineering, is also a promising strategy. Zhang et al. [48] constructed an electrode (labeled 3D-NPG@S-NVO@CTAB) with oxygen vacancies and performed the intercalation of S and CTAB (Figure 3a–c). The density functional theory (DFT) results confirmed that H^+ / Zn^{2+} insertion into MnO_2 containing oxygen defects caused smaller charge depletion regions, suggesting that oxygen defects in MnO_2 were advantageous in terms of enhancing conductivity and boosting charge migration (Figure 3d–f). Xiong et al. [49] employed DFT simulation to assess the oxygen-deficient MnO_2 (Figure 3g). The results showed that Gibbs free energies of Zn^{2+} adsorption near V_O in oxygen-deficient MnO_2 were close to thermoneutral (≈ 0.05 eV), in contrast to pristine MnO_2 , which exhibited much lower values (≈ -3.31 eV).

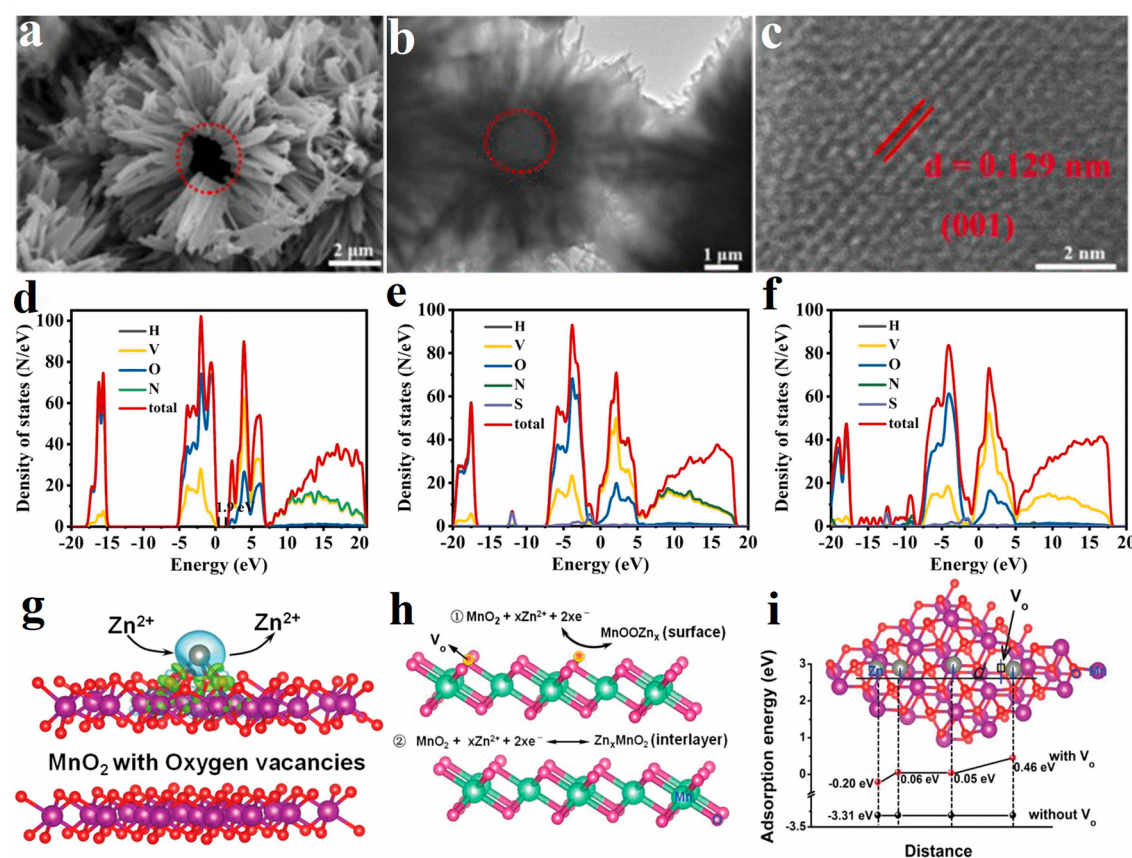


Figure 3. (a) SEM, (b) TEM, and (c) HRTEM images of 3D-NPG@S-NVO@CTAB. The PDOS and TDOS of 3D (d) NPG@NVO, (e) NPG@S-NVO, and (f) NPG@S-NVO@CTAB. Reprinted with permission from ref. [48]. Copyright 2024, Elsevier. Schematic illustrations of (g) Zn^{2+} adsorption/desorption and (h) Zn^{2+} storage on MnO_2 . (i) The calculated Zn^{2+} adsorption energies. Reprinted with permission from ref. [49]. Copyright 2019, Wiley-VCH GmbH.

3. Challenges and Optimization Strategies for Fabrication Techniques of Microelectrodes

It is noticeable that the performance of MBs depends not only on the choice of suitable active materials but also on the design and structure of the fabricated microelectrodes [50]. The electrode architecture of MBs is typically classified into 2D stacked, 2D planar, 3D stacked, 3D planar, and fiber-shaped configurations, which are displayed in Figure 4. Among them, the 2D stacked and planar architectures, which offer the opportunity to construct arbitrarily shaped devices, are the most basic configurations of MBs [51]. Unlike conventional batteries, the fabrication of microelectrodes requires us to address challenges like suitable microprocessing, stable and highly active material loading, and process compatibility [17]. The challenges associated with cathode materials were discussed earlier. Here, the challenges and optimization strategies in the main fabrication techniques are summarized systematically.

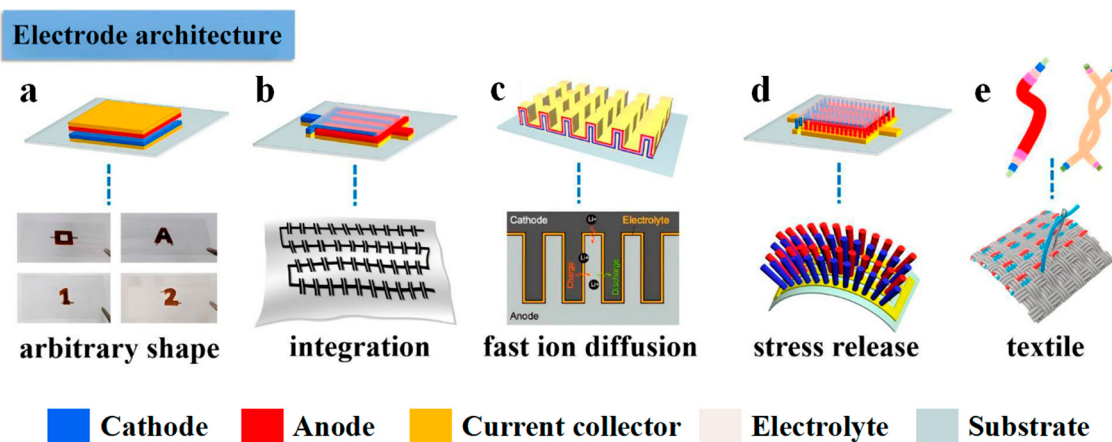


Figure 4. Electrode architectures of MBs and their typical characteristics: (a) 2D stacked; (b) 2D planar; (c) 3D stacked; (d) 3D planar; (e) fiber-shaped. Reprinted with permission from ref. [51]. Copyright 2022, American Chemical Society.

3.1. Challenges in the Fabrication Techniques for Microelectrodes

3.1.1. Low Mass–Loading and Mechanical Instability of Microelectrodes

Currently, commercial MBs are essentially microscale versions of conventional batteries [52]. They typically consist of thin-film electrodes prepared by coating. In this sense, the well-established fabrication method for conventional batteries can be adapted to manufacture MBs cost-effectively. However, the reduction in size results in a reduction in attainable capacity and energy density. As the capacity and energy density are dimension-dependent, they are severely constrained by the limited footprint area of MBs. To some extent, increasing the areal capacity can be accomplished by enhancing the loading mass of the active material. However, this may compromise the stability of the microelectrode during cycling.

3.1.2. The Lack of Facile and Scalable Fabrication Techniques

Unlike with conventional batteries, the construction of MBs requires a miniaturized and compatible approach [53]. The traditional coating method is no longer suitable for fabricating electrodes of MBs. Up until now, several microfabrication technologies, such as lithography, deposition, screen printing, spray coating, laser scribing, and direct ink writing (DIW), have been proposed for the fabrication of microelectrodes. However, those methods have drawbacks, such as high initial costs, poor efficiency, a redundant process, and the low mass loading of active materials. These inherent challenges hinder applications in constructing various microelectrode architectures. For example, owing to the limited space and suboptimal architectural design of microelectrodes, the active material mass loading in screen-printed electrodes is usually very poor and low-resolution. The corresponding strategies for improving those fabrication processes are discussed in Section 3.2.2, respectively.

3.2. Optimization Strategies for Fabrication Techniques of Microelectrodes

3.2.1. Constructing 3D Architecture Microelectrode

Although numerous efforts have been conducted to advance cathode materials with superb performance, the energy density of ZIMBs remains insufficient for practical applications. Apart from the cathode material, the mass loading and structural stability of the microelectrodes also play a crucial role in determining the capacity of ZIMBs. Because of the limited area of 2D geometry, the innovative 3D architecture electrode has emerged. Increasing the mass loading within the constrained footprint area is an effective solution for boosting the energy density of MBs. To this end, 3D architecture electrodes take full

benefit of the vertical dimension (height) to increase the surface-to-volume ratio and enable more mass loading [52]. For example, Naresh et al. [54] introduced porous 3D Au scaffold-based electrodes (IDEs) as current collectors, facilitating the efficient loading of PANI and Zn, respectively (Figure 5a–c). The measured thicknesses of the Zn and PANI for the 3D architecture electrodes are 7 and 17 μm , respectively (Figure 5d), which are much higher than those for flat Au electrodes (6 μm and 11 μm , respectively). In the 3D P-ZIMB, the areal capacities rise from 15 to 35 $\mu\text{Ah cm}^{-2}$ at 50 $\mu\text{A cm}^{-2}$ and from 6.8 to 16 $\mu\text{Ah cm}^{-2}$ at 1000 $\mu\text{A cm}^{-2}$ compared to the C-ZIMB (Figure 5e,f). Even at higher areal currents, the 3D P-ZIMB achieves a substantial enhancement in areal capacity ($\approx 135\%$). Its areal capacities are markedly superior to those of the C-ZIMB (Figure 5g). In general, 3D direct printing is employed to construct 3D electrodes. Printed electrodes were fabricated with 1, 3, and 5 layers, exhibiting proper device formation without any shape distortion. The patterned electrodes reached a maximum height of approximately 2.5 mm with a footprint of around 1.5 cm \times 1.5 cm (Figure 5h) [55]. The printed interdigital electrodes demonstrated good consistency. The optical microscopy of the magnified local view of the electrode reveals the solid electrode's clear formation, featuring sharp corners and clean gaps between interdigital legs. Moreover, interdigital electrodes of various sizes can be accurately manufactured, with the minimum spacing between adjacent electrodes reaching 100 μm (Figure 5i). MBs of varying miniaturized sizes can be efficiently attached to the limited surface area of fingers (Figure 5j), showcasing adjustable miniaturization to suit diverse application needs. The gel-like inks, possessing controlled fluidity, allow for smooth extrusion from the nozzle at a regulated speed, preventing clogging (Figure 5k). Yao et al. [56] demonstrated printed graphene electrodes with high MnO₂ loading (182.2 mg cm^{-2}) (Figure 5l,m), achieving a fairly high areal capacity. Combining picketing emulsion and direct ink writing, Huang et al. developed free-standing, porous polymer foams (Figure 5n,o) [57].

3.2.2. Developing Advanced Fabrication Processes

In terms of device configuration, the challenge lies in locally integrating electrode materials into the microsized architecture without causing a short circuit of the two adjacent electrodes [15]. The achievement of high-resolution microelectrode designs requires advanced technologies. The ever-developing fabrication technologies include printing technologies (such as 3D printing, inkjet printing, screen printing, stamping), etching technologies (photolithography, laser scribing, plasma etching), coating strategies (spray coating, vacuum filtration, layer by layer assembly), and deposition technologies (electrolytic deposition, chemical vapor deposition, electrophoretic deposition). The strategies behind fabrication technologies are discussed in detail to support future investigations and the development of efficient microelectrodes.

Printing Technologies

Printing (direct ink writing, inkjet printing, screen printing, 3D printing, stamping, etc.) is a promising technology that allows specific microelectrode patterns to be formed on a substrate by integrating functional material into an ink system [58]. The most important advantages of printing technologies are cost-effectiveness, ease of processing, and the simplicity of mass production and integration. However, the precision of printed designs is greatly affected by the ink's rheological properties and the stencil's sharpness (for screen printing and stamping).

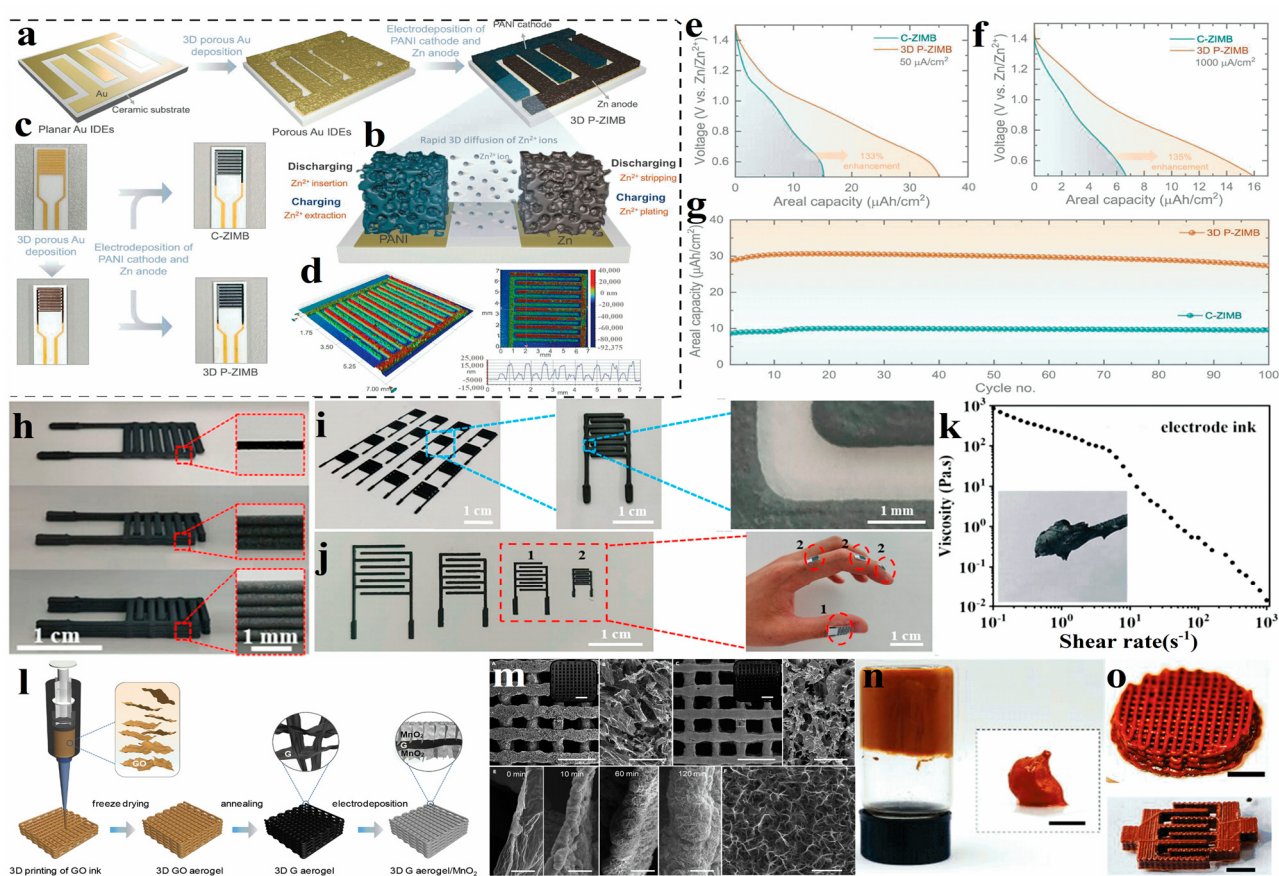


Figure 5. (a) The scheme of the fabrication of 3D P-ZIMBs. (b) A schematic demonstration of the 3D in-plane diffusion. (c) Digital images of the obtained electrodes. (d) 2D and 3D profilometer images of 3D P-ZIMB. GCDs of the C-ZIMB and 3D P-ZIMB at different current densities of (e) $50 \mu\text{A cm}^{-2}$ and (f) $1000 \mu\text{A cm}^{-2}$. (g) The cycling performance of the C-ZIMB and 3D P-ZIMB. Reprinted with permission from ref. [54]. Copyright 2024, Wiley-VCH GmbH. (h) Photos of the interdigital electrodes with 1, 3, and 5 layers, respectively. (i) A photo of the mass fabrication of MBs in a 4×4 layout. (j) Photos of the fabricated MBs in various sizes and their attachment to fingers. (k) Viscosity of the inks as a function of shear rate. Reprinted with permission from ref. [55]. Copyright 2023, American Chemical Society. (l) The fabrication scheme of a 3D-printed electrode. (m) An SEM of a 3D-printed electrode at different magnifications and deposition times. Reprinted with permission from ref. [56]. Copyright 2019, Elsevier. (n) A dispersion consisting of the $\text{V}_2\text{O}_5 \cdot \text{nH}_2\text{O}$ and soybean oil. (o) Photos of 3D-printed emulsified $\text{V}_2\text{O}_5 \cdot \text{nH}_2\text{O}$. Scale bars: 5 mm. Reprinted with permission from ref. [57]. Copyright 2023, Wiley-VCH GmbH.

The 3D printing technique typically involves the optimization of ink properties and printing process parameters. Figure 6a illustrates the printing process [59]. As displayed in Figure 6c, the printed electrode exhibits clear patterns, highlighting the superior printability of the inks. The sheet resistance values of each ink are relatively low (Figure 6d), which facilitates efficient electron transfer. The printed cathode exhibits a mass loading of 14.5 mg cm^{-2} and a thickness of $90 \mu\text{m}$ (Figure 6e). In addition, the magnified SEM image reveals the entanglement between P-NVO and CNTs (Figure 6f). Consequently, printed ZIMBs of 0.95 , 1.42 , and 1.89 cm^2 deliver discharge areal capacities of 3.4 , 3.3 , and 2.9 mAh cm^{-2} at a current density of 2 mA cm^{-2} , respectively (Figure 6b). Moreover, the 3D printing technique offers a potential method for preparing fiber-shaped electrodes (Figure 6g). Various complex patterns (Figure 6h,i) are printed, demonstrating the high accuracy and scalability of the technology.

Screen printing is widely regarded as a usual technique, offering precise control over flexibility, stability, and seamless integration with prepared microelectronics. Wang et al. [60] fabricated Zn//MnO₂ MBs with customizable shapes and intricate planar geometries (Figure 6j,k). To enhance the capacity of ZIMBs, achieving high mass loading while maintaining the structural stability of microelectrodes is crucial. Cai et al. [61] fabricated planar ZIMBs with high energy density by leveraging interfacial engineering. The interlayer, which is composed of hydroxylated carbon nanotube (CNT-OH) and carbon black, preserves the topography intact and significantly improves the mass loading and mechanical stability of microelectrodes. By optimizing the Ce-MnO₂ to CNT-OH ratio and the mass loading, the assembled ZIMBs show an ultra-high capacity (7.2 mAh cm⁻² or 497.3 mAh cm⁻³) and energy density (8.4 mWh cm⁻² or 573.5 mWh cm⁻³), far exceeding those of other similar MBs reported.

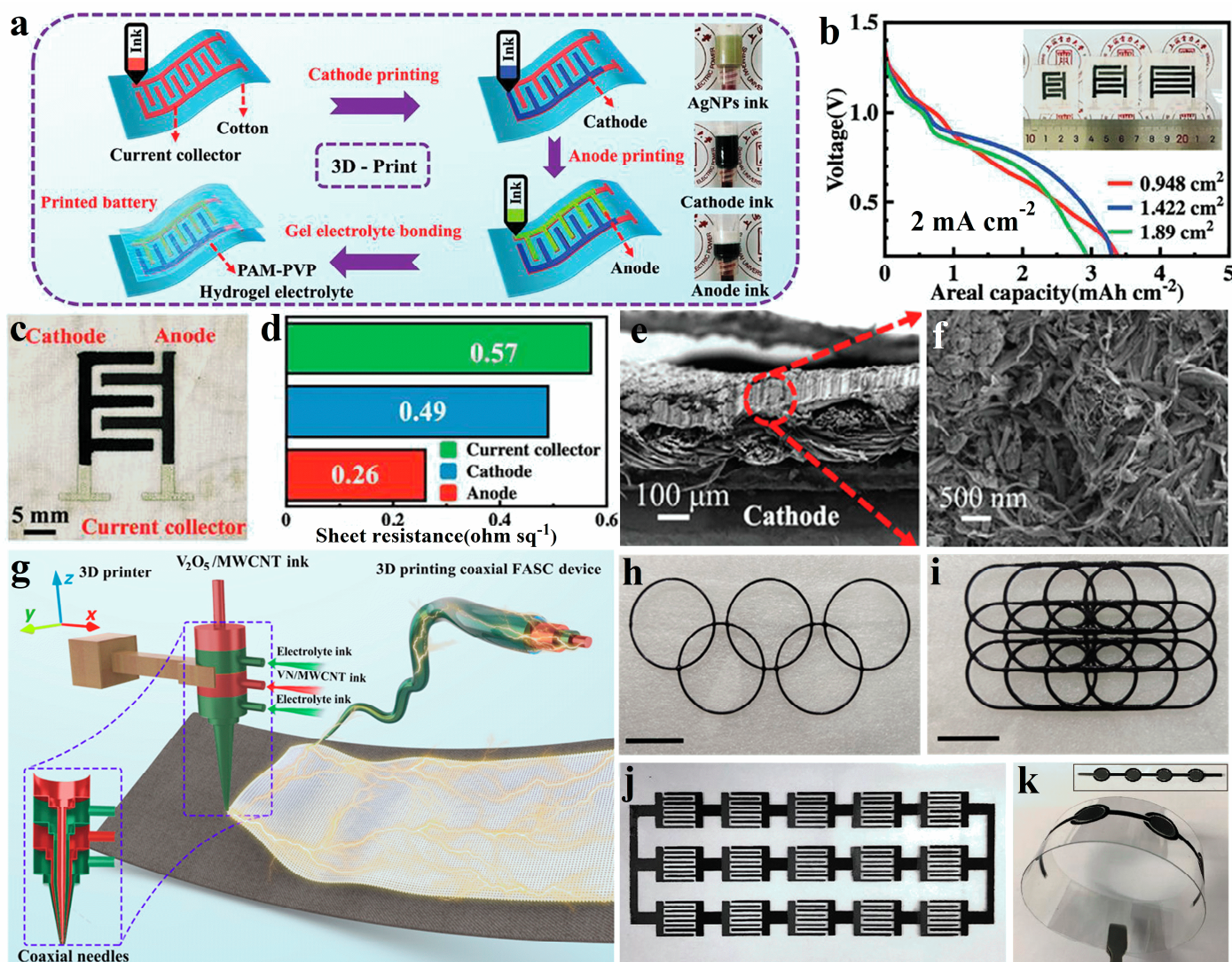


Figure 6. (a) The scheme of the 3D printing process. (b) Discharge curves of PZIMBs with different surface areas at 2 mA cm^{-2} . (c) A photo of and (d) the sheet resistance of the printed electrode. (e) Cross-sectional and (f) surface SEMs of printed cathode. Reprinted with permission from ref. [59]. Copyright 2024, Wiley-VCH GmbH. (g) A coaxial device via direct ink writing. (h,i) The various printed device. Scale bar, 10 mm. Reprinted with permission from ref. [62]. Copyright 2021, the Authors. (j) Zn/MnO_2 MBs connected: 5 series \times 3 parallel. (k) Photos of four concentric circle shapes under a bending state. Reprinted with permission from ref. [60]. Copyright 2019, Oxford University Press.

Etching Technologies

Etching technologies are used to carve high-resolution patterns for the development of on-chip MBs. Laser scribing offers superiority in terms of preparing MBs, including controlled shape and satisfactory accuracy. This is due to the simplicity, scalability, cost-effectiveness, and high-resolution capabilities of the method. The laser beam functions as both a patterning tool and a heat source for carbonization [14]. For instance, Li et al. [63] utilized laser irradiation to construct flexible planar MBs (Figure 7a,b). Owing to the high precision of direct laser patterning technology, the smallest unit is about 2.3 mm^2 ($\approx 1.5\text{ mm} \times 1.5\text{ mm}$) (Figure 7c). Additionally, the width of each finger and the interelectrode gap is only about 160 and 100 μm , respectively. Moreover, it allows for mask-free patterning with arbitrary configurations (Figure 7d).

Coating Technologies

Coating strategies, including layer-by-layer assembly, spray coating, and vacuum filtration, are commonly used to fabricate binder-free thin-film electrodes. These approaches include applying a uniform dispersion onto a substrate, evaporating the dissolvent, and forming a solid film with adjustable thickness. Shadow masks are required to create various patterns, such as interdigital fingers.

Spray coating is widely employed to fabricate microelectrodes. A crucial factor is the ink's ability to produce droplets without causing nozzle clogging during the process. Shi et al. [64] fabricated a planar graphene-based on-chip energy storage device with asymmetric configuration by spray-coating, assisted by a patterned mask on a substrate, as shown in Figure 7e. The device, featuring free-of-metal current collectors, high voltage output, and excellent integration, was very adaptable to on-chip energy devices. To develop a simple and scalable method for the efficient fabrication of fiber-shaped electrodes with high conductivity and mass loading, Lan et al. [65] reported a 3D active coating strategy. In this approach, the active material ink was injected from a stepping syringe onto a rotating conductive wire to create a fiber-shaped electrode (Figure 7f). The as-fabricated fibrous electrode had a diameter of about 670 μm , with a stainless-steel wire as a core. The MnO_2 layer was evenly coated onto the wire's surface and exhibited 235 μm thickness (Figure 7g–i). Accordingly, the weight of coated materials was almost 3.1 mg cm^{-1} or 14.9 mg cm^{-2} , exceeding the mass production demand ($>10\text{ mg cm}^{-2}$).

Vacuum filtration is usually used to fabricate thin films by separating solid materials from liquid. The filtrated film is densely stacked but permeable to ions, resulting in a free-standing electrode with high energy density. Moreover, because of the various dispersions, forming uniform films, including various hybrid materials, is straightforward. The hybridization of high-conductivity carbon materials, like graphene and CNTs, with active materials is a responsible approach for realizing high energy density and superior mechanical properties. For instance, Zhao et al. [66] assembled flexible $\text{MnO}_2@\text{rGO}$ interdigital electrodes, with a thickness of 13.6 μm , using mask-assisted filtration.

Deposition Technologies

As mature methods, deposition technologies have been extensively reported on, including electrolytic deposition, electrophoretic deposition, and chemical vapor deposition (CVD). Microelectrodes can be easily formed by depositing materials on pre-patterned current collectors, thereby eliminating the need for binder additives. The CVD deposition involves high-temperature processing, which thin plastic films (such as PET) are not suitable for. Electrolytic and electrophoretic deposition techniques, on the other hand, are cost-effective and scalable, requiring only simple devices. In these processes, charged nanomaterials are diffused and deposited onto the current collectors under the influence of

electric fields. For instance, Liu et al. [67] constructed an Zn-Mn MB by combining a multi-step electrodeposition technique with laser scribing possesses. Li et al. [68] successfully fabricated a concentric circle structure ZIMB with CNTs/TPU interdigital microelectrodes, where anode Zn and cathode PANI were employed as electrode materials by in situ electrodeposition (Figure 7j). Although deposition is facile and cost-effective, the preparation of MB arrays requires specialized consideration. In addition, the lateral growth of active materials is able to bridge the interval between adjacent electrodes, eventually causing a short circuit. Thus, the concentration of the solution and the time of the process should be arranged accurately. Importantly, the structure of pre-patterned current collectors, which determines the loading of active materials, should be intelligently designed. Wang et al. [69] fabricated a fiber-shaped electrode by electrodepositing MnO₂ onto a carbon fiber rope (CFR) (Figure 7k). The fabricated device exhibited a high power density and energy density, with values of 1.25 mW cm⁻¹ and 0.18 mWh cm⁻¹, respectively.

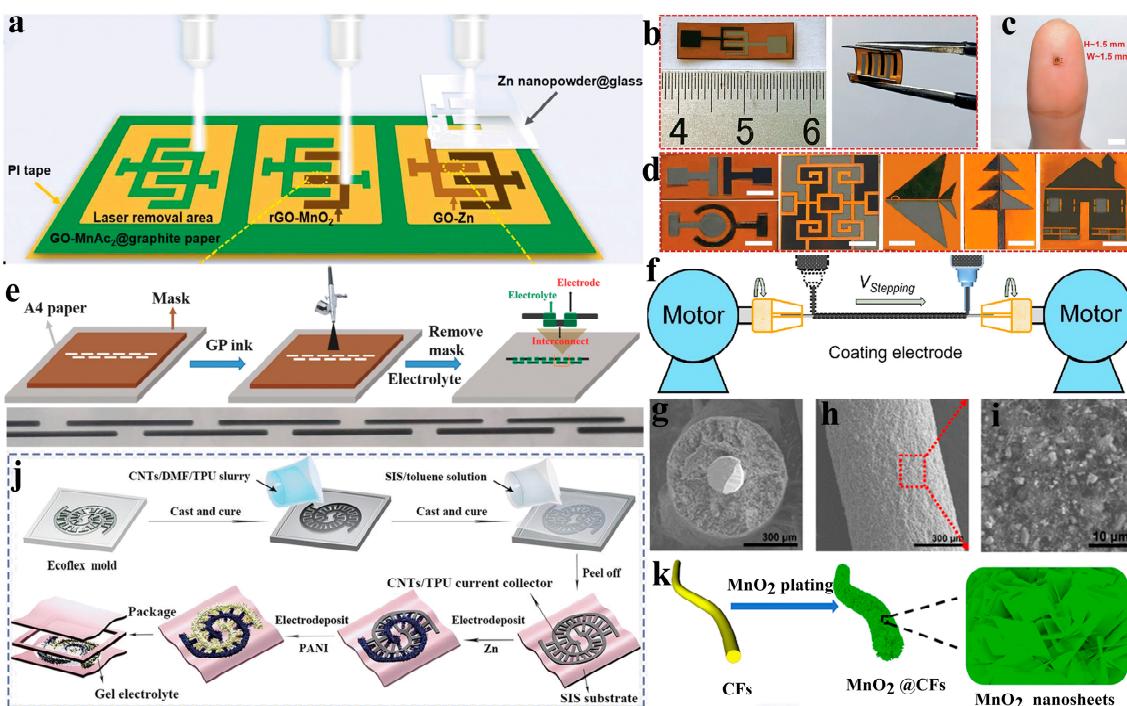


Figure 7. (a) A schematic diagram of the fabrication of MBs. (b) Photos of an MB with planar and bending. (c) An MB on the thumb-scale bar: 5 mm. (d) The various shapes of MBs by all DLP-scale bar: 3 mm. Reprinted with permission from ref. [63]. Copyright 2023, Wiley-VCH GmbH. (e) A schematic diagram and photo of GP-LTMSs. Reprinted with permission from ref. [64]. Copyright 2017, Wiley-VCH GmbH. (f) The scheme for fabricating fibrous batteries. (g–i) An SEM of the fibrous MnO₂ electrodes. Reprinted with permission from ref. [65]. Copyright 2022, American Chemical Society. (j) Schematic diagrams of the processes for Zn-PANI MB. Reprinted with permission from ref. [68]. Copyright 2020, Wiley-VCH GmbH. (k) A schematic diagram of the manufacturing of an MnO₂@CFs electrode. Reprinted with permission from ref. [69]. Copyright 2023, American Chemical Society.

In conclusion, various fabrication techniques have been explored to realize MBs. The efficacy of fabrication techniques can be evaluated in terms of cost, scalability, resolution, multi-material capability, and so on. A comparison of each technique is presented in Table 1.

Table 1. Comparisons of different fabrication techniques used for ZIMBs.

Categories	Technologies	Advantages	Disadvantages
Printing technologies	Screen printing	Fast fabrication, scalable, cost-effective	Low resolution, functional ink-incompatible
	Direct ink writing	Low cost, easy operation, high resolution, material diversity	Strict requirements for viscosity inks (rheological and viscoelastic properties), small-scale production, nozzle jam
Etching technologies	Laser scribing	Fast fabrication, high resolution, scalable, eco-friendly	Expensive equipment
	Photolithography	Cost-effective, high resolution	Harsh work environment
	Plasma etching	Facile	Limited to carbon materials
Coating technologies	Spray coating	Material diversity, scalable, easy operation	Poor homogeneity of the film
	Vacuum filtration	Low cost, facile, controllable thickness	Time-consuming, complex architectures inadaptability
	Layer-by-layer assembly	Material-saving, facile	Complex preparation procedure
Deposition technologies	Electrolytic deposition	Low cost, fast fabrication, scalable, eco-friendly	Uncontrollable growth in a lateral direction
	Electrophoretic deposition	Low cost, simple equipment	Limited to the charged materials
	Chemical vapor deposition	Scalable, controllable thickness	High cost, complicated operation

4. Multiple Applications of ZIMBs

In recent years, there has been a boom in ZIMBs, with varied architectures and cathodes, because of their virtues of outstanding safety and high energy density [70]. Based on the electrode architectures seen in a single device, ZIMBs can usually be classified into three categories: one-dimensional (1D) (which are also named fiber-shaped), two-dimensional (2D), and three-dimensional (3D) designs [17]. Here, we will discuss the application of ZIMBs with different configurations and various performance metrics.

4.1. Fiber-Shaped ZIMBs

Recently, fiber-shaped ZIMBs, with the advantages of bending, twisting, and folding, have been widely studied for their potential application in wearable microelectronics. Using the wet spinning method, Gao et al. [71] assembled flexible 1D ZIMBs with fabricated electrodes. Benefiting from the synergistic effects of both CNTs and CNFs, the fabricated fiber-shaped electrodes demonstrated excellent mechanical properties and desirable conductivity. Combined with the active material MnO_2 , the fiber-shaped ZIMBs demonstrated high volumetric and gravimetric energy densities of $131.3 \text{ mWh cm}^{-3}$ and 47.3 Wh kg^{-1} , respectively. Their high retention capacity, detected after thousands of bending tests, demonstrated their excellent flexibility and structural stability. Consequently, the 1D ZIMBs can be woven into multitudinous structures, such as textiles, in order to power various electronics and achieve various intelligent functions (Figure 8a). Analogously, Zhao et al. [62] fabricated an on-chip coaxial fiber-shaped battery using direct multi-ink writing. The device delivered excellent areal energy and power density during the high loading of active materials and demonstrated outstanding stability (Figure 8b). Xia et al. [72] fabri-

cated a wearable self-powered device by integrating a solar cell with a fiber-shaped battery to provide power for an electronic watch (Figure 8c). The solar charging-discharging test lasted for about 4 h and demonstrated outstanding repeatability.

In terms of device configuration, fiber-shaped ZIMBs can be classified into coaxial, twisted, and parallel types. First, the coaxial configuration features a hollow multi-shell or core–shell configuration, where the anode and cathode share the same axis. The configuration is more compact and has higher ion transfer efficiency. Zhang et al. [73] reported on coaxial ZIMBs that were integrated with a strain sensor (Figure 8d–f). Second, the twisted configuration included two-line-electrode-coated gel electrolytes, which were twisted into a double helix structure. Li et al. [74] synthesized a Ni-V₂O₅ NWs@CNT fiber electrode by a novel quenching method (Figure 8g), and then assembled fiber-shaped ZIMBs by twisting the Ni-V₂O₅ NWs@CNT cathode fiber and Zn NSs@CNT anode fiber, which were coated with gel electrolyte. Moreover, the fiber-shaped ZIMBs continued to perform well when knitted into a textile glove (Figure 8h). With their integration into a soft robot, it was able to operate in an untethered way and move forward (Figure 8i). Third, for the parallel configuration, the anodes were arranged in parallel to the cathode, with a separator or electrolyte in between (Figure 8j) [75]. The as-fabricated fiber-shaped battery was integrated with a wearable NO₂ gas sensor (Figure 8l) and pressure sensor (Figure 8k) for application.

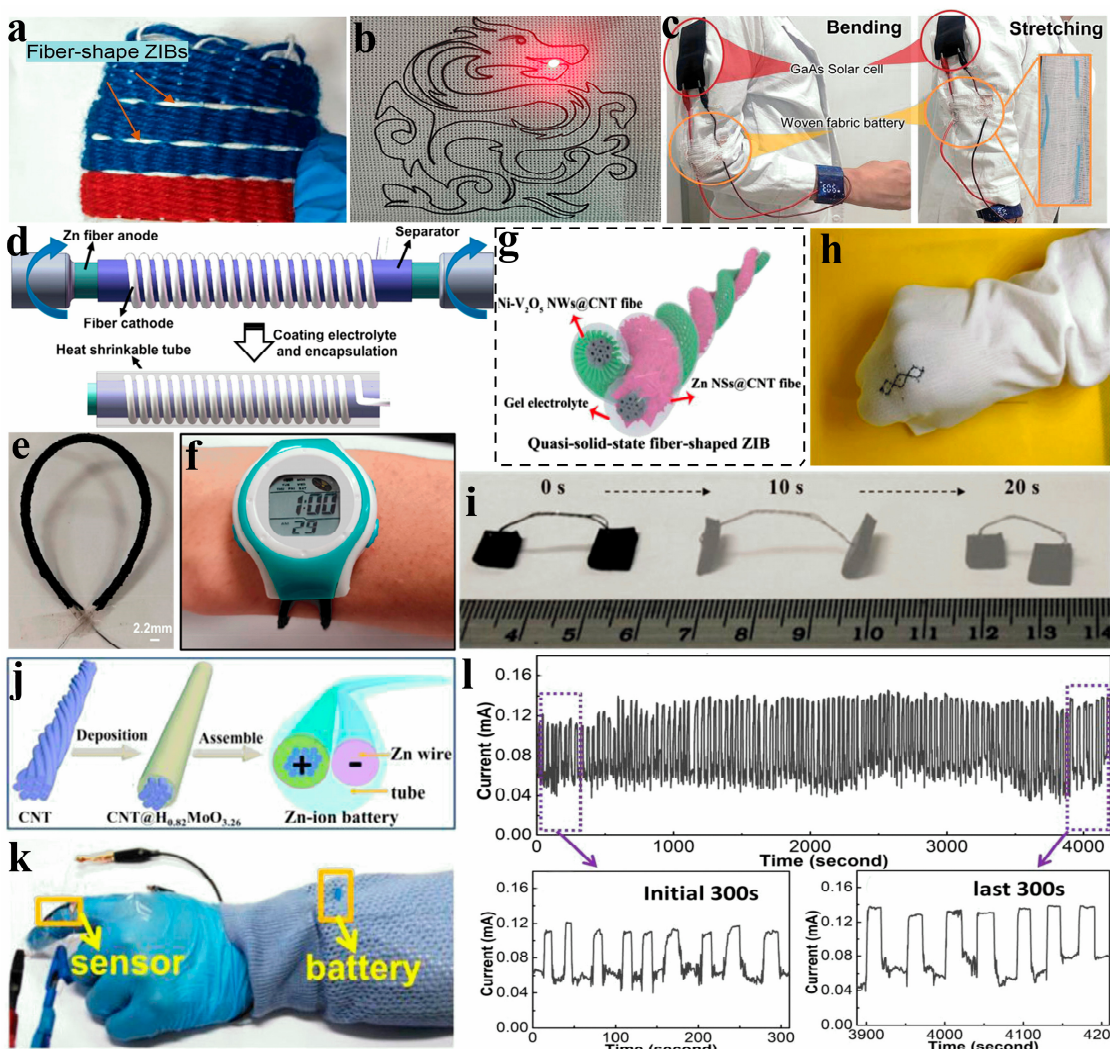


Figure 8. (a) A photo of a textile woven with the fiber-shaped ZIMBs. Reprinted with permission from ref. [71]. Copyright 2022, Elsevier. (b) A photo of an LED illuminated by a coaxial device.

Reprinted with permission from ref. [62]. Copyright 2021, the authors. (c) A photo of a wearable self-power integrated system. Reprinted with permission from ref. [72]. Copyright 2021, Copyright 2022, Wiley-VCH GmbH. (d) The preparation process of a multifunctional battery. (e) A photo of the fiber-shaped device. (f) A photo of an electronic watch driven by two fiber-shaped devices in series. Reprinted with permission from ref. [73]. Copyright 2022, American Chemical Society. (g) A schematic illustration of the fiber-shaped battery. (h) A photo of the fiber-shaped battery woven into a textile. (i) Robotic locomotion under magnetic actuation. Reprinted with permission from ref. [74]. Copyright 2022, Elsevier. (j) A schematic diagram of the fabricated fiber electrode and fiber-shaped ZIMBs. (k) A photo of the integrated device used to monitor the movement. (l) The dynamic response of the sensor with the finger moving. Reprinted with permission from ref. [75]. Copyright 2022, Elsevier.

4.2. Two-Dimensional (2D) ZIMBs

At present, two-dimensional (2D) ZIMBs are classified into 2D staked configurations and 2D interdigital configurations, both of which are commonly accepted for assembling microdevices. Normally, the 2D staked configuration has a sandwich-like structure that follows traditional battery design principles. In the early stage, a Zn / MnO₂ MB with a gel electrolyte was developed through direct write printing and this was easily integrated onto the substrate [76].

Since the application of gel electrolytes in electrochemical energy storage devices, the development of rechargeable ZIMBs has advanced significantly. Zeng et al. [77] designed a high-performance quasi-solid-state ZIMB. Owing to the buffer layer of PEDOT and the Mn²⁺ neutral electrolyte, the ZIMB achieved admirable energy density and peak power density values of 34 mW h cm⁻³ and 8.6 kW kg⁻¹, respectively. Recently, Zheng et al. [78] presented a novel zinc ion gel (Zn-gel) electrolyte, synthesized via the ethanol vapor-induced assembly of cellulose molecules, applied to ZIMBs (Figure 9a,b). The Zn-gel showed exceptional mechanical strength (0.88 MPa), high ion transference (over 0.7), and superior ionic conductivity (8.39 mS cm⁻¹). The ZIMB with Zn-gel achieved a capacity of 207.3 mAh g⁻¹ and coulombic efficiency over 93% after 500 cycles without a liquid electrolyte. These highly safe and wearable ZIMBs provided dependable performances under harsh conditions. To enhance lifetimes and solve safety issues, an anti-freezing, self-healing MB was proposed with the help of a cross-linked polyacrylamide polyelectrolyte (Figure 9c-f) [79]. This electrolyte efficiently improved the lifespan and widened the working temperature range.

In 2D interdigital ZIMBs, separated parallel electrodes are arranged on an all-in-one substrate, allowing for speedy and multidirectional ion diffusion without a separator. Thus far, a number of investigations have concentrated on optimizing the structural design of microelectrodes so as to shorten ion transport paths and achieve high power density. Typically, ZIMBs have been exploited by engraving free-standing VO₂-MWCNTs and zinc nanosheets into interdigital electrodes with facile, cost-efficient, and high-resolution laser engraving [80]. The ZIMB exhibited a splendid ultrahigh capacity, energy density, and power density of 315 µAh cm⁻², 189 µWh cm⁻², and 0.6 mW cm⁻², respectively. Moreover, the ZIMB also demonstrated excellent high temperature stability and mechanical flexibility. Meanwhile, the authors constructed interdigital A-V₂O₅/G-ZIMBs, with Zn powder as the anode and a 2D A-V₂O₅/G heterostructure film (7 µm) as the cathode, on an all-in-one substrate via a mask-assisted vacuum filtration strategy [81]. They demonstrated an ultra-high volumetric capacity of 20 mAh cm⁻³ at a current density of 1 mA cm⁻² and the model retained 80% of its capacity after 3500 cycles. For integrated application, Zhang [82] printed sweat-activated Zn/MoS₂-MnO₂ micro-batteries, suitable for power supply modules in long-duration wearables (Figure 9g,h). Analogously, Lu et al. [59] fabricated an interactive integrated system resembling electronic skin (Figure 9i). To ensure reliability and integrability for wearable product applications, stretchable ZIMBs were

fabricated by incorporating conductive polymer intercalated vanadium oxide in flexible and elastic cathode materials [83]. The as-fabricated ZIMBs showed superior stretchability (500% of the pristine length) (Figure 9j) and temperature adaptability (-20 to 60 $^{\circ}\text{C}$) (Figure 9k). Obviously, the ZIMBs could adapt to extreme environments.

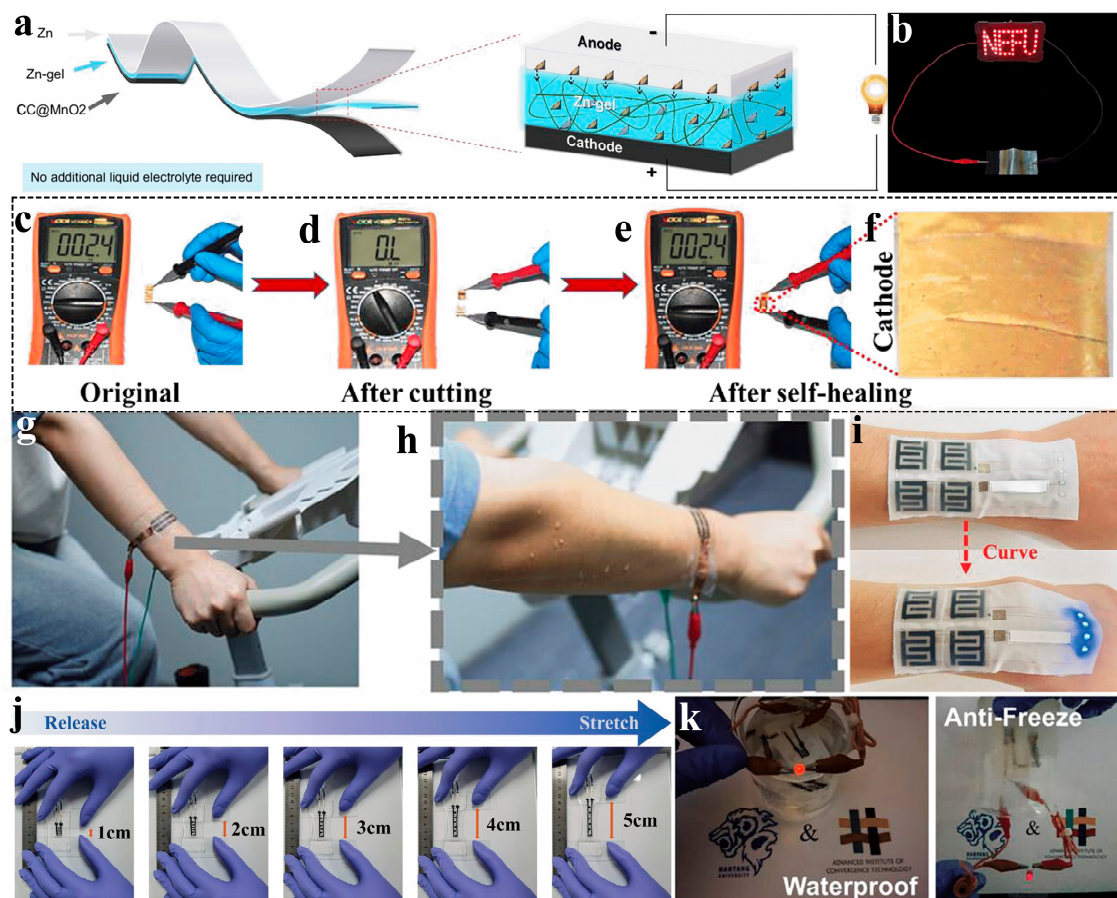


Figure 9. (a) A schematic diagram of a stacked ZIB. (b) A photo of a ZIB providing power for LED under bending. Reprinted with permission from ref. [78]. Copyright 2024, Wiley-VCH GmbH. (c–f) The resistance variation of the cathode before cutting and after self-healing. Reprinted with permission from ref. [79]. Copyright 2022, Elsevier. (g,h) A photo of on-body trial setup with the Zn/MoS₂-MnO₂ batteries mounted on the arm while riding an exercise bike. Reprinted with permission from ref. [82]. Copyright 2024, Wiley-VCH GmbH. (i) A photo of an interactive integrated system resembling electronic skin. Reprinted with permission from ref. [59]. Copyright 2024, Wiley-VCH GmbH. (j) Photos of ZIMBs while stretched up to 5 cm. (k) LED illumination using a ZIMB in water and ice. Reprinted with permission from ref. [83]. Copyright 2023, Wiley-VCH GmbH.

4.3. Three-Dimensional (3D) ZIMBs

To mitigate the low energy density of 2D ZIMBs, 3D ZIMBs are proposed. Among the multitudinous configurations, the interdigitated conformation is the most typical due to its high aspect ratios, which allows for high mass loadings [14]. With the development of printing techniques, various 3D microelectrodes are constructed layer by layer through printing. Yao et al. [76] demonstrated a 3D-printed electrode with MnO₂ mass loading up to 182 mg cm^{-2} , achieving a high areal capacity. In addition, these series devices can power an LED (Figure 10a), proving their feasibility in practical applications. An energy supply module consisting of four single MBs, connected in series and parallel, is used to power a miniature motor (Figure 10b) [55], demonstrating strong and durable powering capability. Li et al. [68] fabricated a flexible Zn- PANI MB with a concentric

circle structure. The device, integrated with three MBs, can easily power a digital watch on the wrist (Figure 10c), exhibiting excellent flexibility and wearability. Shi et al. [84] fabricated all-printed 3DP-Cu@Gr//MnO₂ ZIMBs (Figure 10d). Benefiting from the 3D architecture with customizable geometries, which was beneficial to the reversible cycling of Zn metal, the as-fabricated device demonstrated up to 91.4% capacity retention and almost 100% coulombic efficiency after 200 cycles (Figure 10e). In addition, the high energy density and power density were 48.6 Wh kg⁻¹ and 18.8 W kg⁻¹, respectively. Obviously, the combination of energy/current output, cycle life, and flexibility is extremely favorable. Meng et al. [85] utilized surface path planning techniques with five-axis linkage technology, which expanded the printing capabilities to non-deployable surfaces. A conformal curved surface functional integrated circuit, including a Zn//MnO₂ cell module, a nano-silver temperature sensor, and a conductive pathway, is displayed in Figure 10f. The printing process enables the conformal fabrication of functional circuits, making it suitable for applications with space constraints and laying the groundwork for the miniaturization and conformal production of self-power wearable electronics.

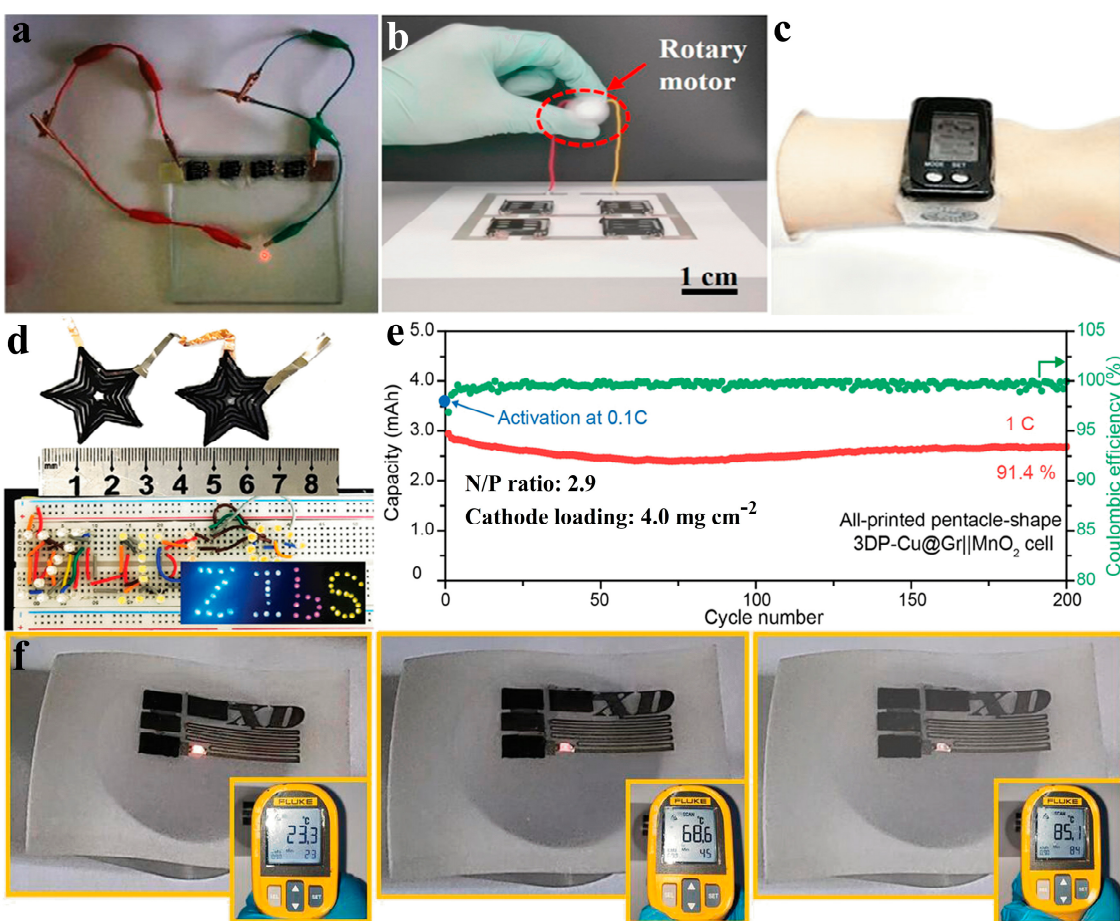


Figure 10. (a) A photo of four devices, in series, lighting an LED. Reprinted with permission from ref. [57]. Copyright 2023, Wiley-VCH GmbH. (b) A module with four individual devices powers a miniature rotary motor. Reprinted with permission from ref. [55]. Copyright 2023, American Chemical Society. (c) A watch is powered by three MBs in series. Reprinted with permission from ref. [68]. Copyright 2020, Wiley-VCH GmbH. (d) Photo and (e) cycle performance of all printed AZIBs. Reprinted with permission from ref. [84]. Copyright 2024, Wiley-VCH GmbH. (f) Temperature change test of conformal temperature measurement circuit. Reprinted with permission from ref. [85]. Copyright 2024, Wiley-VCH GmbH.

5. Conclusions and Prospects

Considering their features, such as large abundance, low cost, environmental sustainability, and being nontoxic, as well as the low redox potential of the Zn anode, ZIMBs are promising micropower sources for wearable electronics and smart devices. To achieve extended cycle life, superior energy density, and remarkable power density within a limited footprint, it is crucial to enhance key components, particularly the cathode. This requires the use of high-capacity active materials. Significant endeavors have been undertaken to explore advanced cathode materials and develop microelectrodes to meet these demands. This review provides a comprehensive analysis of the challenges faced by researchers and possible strategies for future research and advancement, from the perspectives of material design, electrode fabrication, and structural configurations for ZIMBs. Additionally, the applications of ZIMBs in powering electronics, like wearable devices, flexible robots, and sensors, are discussed. Despite the tremendous advancements that have been made in the advancement of novel active materials and the design of intelligent microelectrode architectures, many challenges remain in meeting the requirements for application in flexible wearable devices, flexible robots, and micro-sensors.

- (1) Challenges persist in relation to cathode materials. In order to output more capacity in a limited space, the bulk energy density of the material must be prioritized. The materials' vibration density or compactness should also be given greater attention. Electrode materials based on conversion or redox reaction mechanisms are likely to be more promising due to their higher energy density. Additionally, the structure of electrodes is different, and the factors restricting the performance of the battery are different. The proportion of conductive additives in an electrode of a few microns thick may not improve the performance of the MB but rather reduce the specificity of the MB. Therefore, it is very important to achieve a better understanding of the material's electrochemical mechanisms and restriction factors in MB architectures by advanced *in situ* or *operando* characterization techniques.
- (2) Challenges persist in relation to cost-effective, time-efficient, accessible, scalable, and compatible fabrication techniques. The architectures of microelectrodes are essential for the energy/power density and operational stability of ZIMBs. Although various innovative fabrication methods, such as photolithography, deposition, laser scribing, and filtration, have been developed to fabricate microelectrodes, each of these methods has its respective advantages and drawbacks. Most current downsizing approaches are complex, tedious, and limited to lab-scale production. Research on developing facile and efficient approaches for large-scale and cost-effective fabrication techniques is therefore urgently needed for the commercialization of ZIMBs. Among the available methods, printing is widely regarded as a promising candidate. However, there is a shortage of suitable inks with excellent rheological properties that combine conductive materials and active materials. To date, only a few printable inks have been developed based on active materials. Consequently, significant efforts should be focused on the creation of such printable inks. Additionally, achieving a high printing resolution remains a key challenge for the future development of printing techniques. Advancements in resolution would enable the fabrication of electrode architectures with more precise and adaptable structures. The ultimate goal of this technology is to realize fully printed micro-batteries (MBs), where all components, such as anode, the cathode, electrolyte, separator, and current collectors, can be printed simultaneously. Furthermore, constructing a complete fabrication database based on current fabrication techniques is of great significance, as it would offer crucial direction and guidance to users. As far as the fabrication methods are concerned, we can attempt to combine multiple methods, utilizing their respective advantages to

advance high-performance ZIMBs. For instance, it is possible to achieve electrodes with a 3D porous structure by directly ink printing the active material, followed by laser scribing.

- (3) Innovative configuration design. The strategy of choosing suitable electrode materials, fabrication techniques, and innovative configuration designs could lay the foundation for the development of high-performance ZIMBs. With the advancement of technical readiness, 2D microelectrodes with planar and stacked architectures are progressively transitioning to 3D planar and stacked architectures, offering high areal energy and power densities within a limited footprint. However, successfully transitioning ZIMBs with architectures of 3D electrodes from the laboratory stage to commercialization remains a challenging task. A number of challenges must be addressed, including the further optimization of performance, development of scalable and cost-effective fabrication methods, complete and uniform electrolyte filling, and the compatible integration of ZIMBs with microdevices.

Author Contributions: L.D. and T.W.: original draft preparation; L.D., Z.L. and Q.L.: formatting and graphics; K.S., T.W. and J.C.: review and editing; funding acquisition. All authors have read and agreed to the published version of the manuscript.

Funding: This work was supported by the National Natural Science Foundation of China (No. 52202307, 52402313), the Science and Technology Innovation Program of Hunan Province (No. 2021RC5007) and the Natural Science Foundation of Hunan Province (No. 2022JJ40447, 2023JJ50479). Guangdong Basic and Applied Basic Research Foundation (2021A1515110347, 2022A1515111170). The Xiangtan City Science and Technology Plan Project (GX-YB20231008). The Key Project of Xiangtan Municipal Science and Technology Bureau (No. ZX-ZD20240001).

Conflicts of Interest: The authors declare no conflict of interest.

References

- Zhu, X.; Zhang, H.; Huang, Y.; He, E.; Shen, Y.; Huang, G.; Yuan, S.; Dong, X.; Zhang, Y.; Chen, R.; et al. Recent progress of flexible rechargeable batteries. *Sci. Bull.* **2024**, *69*, 3730–3755. [[CrossRef](#)]
- Liu, S.; Yang, J.; Chen, P.; Wang, M.; He, S.; Wang, L.; Qiu, J. Flexible Electrodes for Aqueous Hybrid Supercapacitors: Recent Advances and Future Prospects. *Electrochem. Energy Rev.* **2024**, *7*, 25. [[CrossRef](#)]
- Tang, L.; Peng, H.; Kang, J.; Chen, H.; Zhang, M.; Liu, Y.; Kim, D.H.; Liu, Y.; Lin, Z. Zn-based batteries for sustainable energy storage: Strategies and mechanisms. *Chem. Soc. Rev.* **2024**, *53*, 4877–4925. [[CrossRef](#)] [[PubMed](#)]
- Zhu, M.; Schmidt, O.G. Tiny robots and sensors need tiny batteries—Here's how to do it. *Nature* **2021**, *589*, 195. [[CrossRef](#)]
- Xiao, X.; Zheng, Z.; Zhong, X.; Gao, R.; Piao, Z.; Jiao, M.; Zhou, G. Rational Design of Flexible Zn-Based Batteries for Wearable Electronic Devices. *ACS Nano* **2023**, *17*, 1764–1802. [[CrossRef](#)] [[PubMed](#)]
- Qu, Z.; Zhu, M.; Tang, H.; Liu, L.; Li, Y.; Schmidt, O.G. Towards high-performance microscale batteries: Configurations and optimization of electrode materials by in-situ analytical platforms. *Energy Storage Mater.* **2020**, *29*, 17–41. [[CrossRef](#)]
- Ma, J.; Zheng, S.; Das, P.; Lu, P.; Yu, Y.; Wu, Z.-S. Sodium Ion Microscale Electrochemical Energy Storage Device: Present Status and Future Perspective. *Small Struct.* **2020**, *1*, 2000053. [[CrossRef](#)]
- Pam, M.E.; Yan, D.; Yu, J.; Fang, D.; Guo, L.; Li, X.L.; Li, T.C.; Lu, X.; Ang, L.K.; Amal, R.; et al. Microstructural Engineering of Cathode Materials for Advanced Zinc-Ion Aqueous Batteries. *Adv. Sci.* **2020**, *8*, 2002722. [[CrossRef](#)]
- Li, X.; Wang, L.; Fu, Y.; Dang, H.; Wang, D.; Ran, F. Optimization strategies toward advanced aqueous zinc-ion batteries: From facing key issues to viable solutions. *Nano Energy* **2023**, *116*, 108858. [[CrossRef](#)]
- Li, G.; Sun, L.; Zhang, S.; Zhang, C.; Jin, H.; Davey, K.; Liang, G.; Liu, S.; Mao, J.; Guo, Z. Developing Cathode Materials for Aqueous Zinc Ion Batteries: Challenges and Practical Prospects. *Adv. Funct. Mater.* **2023**, *34*, 2301291. [[CrossRef](#)]
- Javed, M.S.; Najam, T.; Hussain, I.; Idrees, M.; Ahmad, A.; Imran, M.; Shah, S.S.A.; Luque, R.; Han, W. Fundamentals and Scientific Challenges in Structural Design of Cathode Materials for Zinc-Ion Hybrid Supercapacitors. *Adv. Energy Mater.* **2022**, *13*, 2202303. [[CrossRef](#)]
- Xu, X.; Chen, Y.; Li, W.; Yin, R.; Zheng, D.; Niu, X.; Dai, X.; Shi, W.; Liu, W.; Wu, F.; et al. Achieving Ultralong-Cycle Zinc-Ion Battery via Synergistically Electronic and Structural Regulation of a MnO₂ Nanocrystal-Carbon Hybrid Framework. *Small* **2023**, *19*, e2207517. [[CrossRef](#)] [[PubMed](#)]

13. Wang, J.; Liu, B.; Wang, Z.; Liu, Z.; Li, L.; Wang, M.; Meng, X.; Yong, Y.; Wang, H.; Yin, Z. Synergistic Phase and Structural Engineering for Enhanced Zinc Storage in V₂O₃@N-Doped Carbon Nanofibers. *Small* **2024**, e2410380. [CrossRef] [PubMed]
14. Chen, F.; Xu, Z.-L. Design and manufacture of high-performance microbatteries: Lithium and beyond. *Microstructures* **2022**, *2*, 2022012. [CrossRef]
15. Kyeremateng, N.A.; Brousse, T.; Pech, D. Microsupercapacitors as miniaturized energy-storage components for on-chip electronics. *Nat. Nanotechnol.* **2017**, *12*, 7–15. [CrossRef] [PubMed]
16. Li, Y.; Xiao, S.; Qiu, T.; Lang, X.; Tan, H.; Wang, Y.; Li, Y. Recent advances on energy storage microdevices: From materials to configurations. *Energy Storage Mater.* **2022**, *45*, 741–767. [CrossRef]
17. Moghadami, M.; Massoudi, A.; Nangir, M. Unveiling the recent advances in micro-electrode materials and configurations for sodium-ion micro-batteries. *J. Mater. Chem. A* **2024**, *12*, 17923–17957. [CrossRef]
18. Huang, J.; Wang, Z.; Hou, M.; Dong, X.; Liu, Y.; Wang, Y.; Xia, Y. Polyaniline-intercalated manganese dioxide nanolayers as a high-performance cathode material for an aqueous zinc-ion battery. *Nat. Commun.* **2018**, *9*, 2906. [CrossRef] [PubMed]
19. Guo, S.; Liang, S.; Zhang, B.; Fang, G.; Ma, D.; Zhou, J. Cathode Interfacial Layer Formation via in Situ Electrochemically Charging in Aqueous Zinc-Ion Battery. *ACS Nano* **2019**, *13*, 13456–13464. [CrossRef]
20. Zhao, B.; Jia, P.; Yu, L.; Song, Y.; Li, Z.; Wang, Y.; Feng, R.; Li, H.; Cui, X.; Cui, H.; et al. Cathode materials for aqueous zinc-ion batteries and prospect of self-supporting electrodes: A review. *J. Energy Storage* **2023**, *73*, 109174. [CrossRef]
21. Liu, M.; Wang, P.; Zhang, W.; He, H.; He, G.; Xu, S.; Yao, L.; Miller, T.S. Strategies for pH regulation in aqueous zinc ion batteries. *Energy Storage Mater.* **2024**, *67*, 103248. [CrossRef]
22. Yang, J.; Yin, B.; Sun, Y.; Pan, H.; Sun, W.; Jia, B.; Zhang, S.; Ma, T. Zinc Anode for Mild Aqueous Zinc-Ion Batteries: Challenges, Strategies, and Perspectives. *Nanomicro Lett.* **2022**, *14*, 42. [CrossRef] [PubMed]
23. Wan, G.; Sun, W.; Liu, L.; Mao, C.; Zhang, Z.; Guo, X.; Li, G. Nutrient for Inhibiting the Activity of H₂O and Optimizing Interfacial Chemistry for Aqueous Rechargeable Zn-Ion Batteries. *ACS Sustain. Chem. Eng.* **2024**, *12*, 5475–5483. [CrossRef]
24. Sun, W.; Liu, Y.; Liu, L.; Li, Q.; Liu, X.; Zhang, Z.; Zheng, J.; Guo, X.; Li, G. A “dynamic water microdomain” strategy to manipulate Zn anode reactions. *Chem. Eng. J.* **2024**, *496*, 154101. [CrossRef]
25. Jing, F.; Lv, C.; Xu, L.; Shang, Y.; Pei, J.; Song, P.; Wang, Y.; Chen, G.; Yan, C. An amorphous manganese iron oxide hollow nanocube cathode for aqueous zinc ion batteries. *J. Energy Chem.* **2023**, *87*, 314–321. [CrossRef]
26. Liu, Q.; Fan, G.; Zeng, Y.; Zhang, X.; Luan, D.; Guo, Y.; Gu, X.; Lou, X.W. Hollow Octahedral Pr₆O₁₁-Mn₂O₃ Heterostructures for High-Performance Aqueous Zn-Ion Batteries. *Adv. Energy Mater.* **2024**, *14*, 2402743. [CrossRef]
27. Lin, C.; Zhang, H.; Zhang, X.; Liu, Y.; Zhang, Y. Kinetics-Driven MnO₂ Nanoflowers Supported by Interconnected Porous Hollow Carbon Spheres for Zinc-Ion Batteries. *ACS Appl. Mater. Interfaces* **2023**, *15*, 14388–14398. [CrossRef] [PubMed]
28. Zhao, Q.; Zhang, H.; Wang, X.; Xu, T.; Zhang, M.; Wang, Y.; Zhu, L.; Tong, S.; Zhou, X.; Li, J.; et al. Highly reversible and rapid charge transfer Zn-MnO₂ battery by MnO₂ nanosheet arrays anchored nanocellulose-based carbon aerogel. *Adv. Compos. Hybrid Mater.* **2024**, *7*, 90. [CrossRef]
29. Wang, K.; Liu, X.; Zhao, F.; Zhang, D.; Cui, Y.; Yang, Z.; Li, X.; Zhang, Y.; Su, H.; Wu, J.; et al. Dressing the manganese dioxide cathode with close-fitting thin carbon film to suppress the dissolution and expansion. *Chem. Eng. J.* **2023**, *474*, 145543. [CrossRef]
30. Bie, Z.; Jiao, Z.; Cai, X.; Wang, Z.; Zhang, X.; Li, Y.; Song, W. Pomegranate-Inspired Cathodes Mitigate the Mismatch Between Carrier Transport and High Loading for Aqueous Zinc-Ion Batteries. *Adv. Energy Mater.* **2024**, *14*, 2401002. [CrossRef]
31. Li, N.; Hou, Z.; Liang, S.; Cao, Y.; Liu, H.; Hua, W.; Wei, C.; Kang, F.; Wang, J.-G. Highly flexible MnO₂@polyaniline core-shell nanowire film toward substantially expedited zinc energy storage. *Chem. Eng. J.* **2023**, *452*, 139408. [CrossRef]
32. Ma, Y.; Xu, M.; Huang, S.; Wang, L.; Xiao, H.; Chen, L.; Zhang, Z.; Liu, R.; Yuan, G. Conformal poly 3,4-ethylene dioxythiophene skin stabilized epsilon-type manganese dioxide microspheres for zinc ion batteries with high volumetric energy density. *J. Colloid Interface Sci.* **2023**, *649*, 996–1005. [CrossRef] [PubMed]
33. Jiao, Y.; Kang, L.; Berry-Gair, J.; McColl, K.; Li, J.; Dong, H.; Jiang, H.; Wang, R.; Corà, F.; Brett, D.J.L.; et al. Enabling stable MnO₂ matrix for aqueous zinc-ion battery cathodes. *J. Mater. Chem. A* **2020**, *8*, 22075–22082. [CrossRef]
34. Gao, X.; Shen, C.; Dong, H.; Dai, Y.; Jiang, P.; Parkin, I.P.; Zhang, H.; Carmalt, C.J.; He, G. Co-intercalation strategy for simultaneously boosting two-electron conversion and bulk stabilization of Mn-based cathodes in aqueous zinc-ion batteries. *Energy Environ. Sci.* **2024**, *17*, 2287–2297. [CrossRef]
35. Jing, F.; Liu, Y.; Shang, Y.; Lv, C.; Xu, L.; Pei, J.; Liu, J.; Chen, G.; Yan, C. Dual ions intercalation drives high-performance aqueous Zn-ion storage on birnessite-type manganese oxides cathode. *Energy Storage Mater.* **2022**, *49*, 164–171. [CrossRef]
36. Li, Z.; Deng, L.; Wei, T.; Zhao, H.; Wang, C.; Wei, X. Laser-induced oxygen vacancy defect Mn₇O₁₃·5H₂O as binder-free cathode for high performance all-in-one zinc-ion battery. *Appl. Surf. Sci.* **2023**, *639*, 158219. [CrossRef]
37. Long, F.; Xiang, Y.; Yang, S.; Li, Y.; Du, H.; Liu, Y.; Wu, X.; Wu, X. Layered manganese dioxide nanoflowers with Cu²⁺ and Bi³⁺ intercalation as high-performance cathode for aqueous zinc-ion battery. *J. Colloid Interface Sci.* **2022**, *616*, 101–109. [CrossRef]
38. Wang, K.; Wang, J.; Chen, P.; Qin, M.; Yang, C.; Zhang, W.; Zhang, Z.; Zhen, Y.; Fu, F.; Xu, B. Structural Transformation by Crystal Engineering Endows Aqueous Zinc-Ion Batteries with Ultra-long Cyclability. *Small* **2023**, *19*, e2300585. [CrossRef]

39. Ma, Y.; Xu, M.; Liu, R.; Xiao, H.; Liu, Y.; Wang, X.; Huang, Y.; Yuan, G. Molecular tailoring of MnO_2 by bismuth doping to achieve aqueous zinc-ion battery with capacitor-level durability. *Energy Storage Mater.* **2022**, *48*, 212–222. [CrossRef]
40. Wang, X.; Wang, Y.; Naveed, A.; Li, G.; Zhang, H.; Zhou, Y.; Dou, A.; Su, M.; Liu, Y.; Guo, R.; et al. Magnesium Ion Doping and Micro-Structural Engineering Assist $\text{NH}_4\text{V}_4\text{O}_{10}$ as a High-Performance Aqueous Zinc Ion Battery Cathode. *Adv. Funct. Mater.* **2023**, *33*, 2306205. [CrossRef]
41. Cai, X.; Zhang, Y.; Cheng, H.; Liu, C.; Wang, Z.; Ye, H.; Pan, Y.; Jia, D.; Lin, H. Polypyrrole-Doped $\text{NH}_4\text{V}_3\text{O}_8$ with Oxygen Vacancies as High-Performance Cathode Material for Aqueous Zinc-Ion Batteries. *Small* **2023**, *19*, e2304668. [CrossRef] [PubMed]
42. Chen, H.; Ma, W.; Guo, J.; Xiong, J.; Hou, F.; Si, W.; Sang, Z.; Yang, D. PEDOT-intercalated MnO_2 layers as a high-performance cathode material for aqueous Zn-ion batteries. *J. Alloys Compd.* **2023**, *932*, 167688. [CrossRef]
43. Deng, L.; Sun, K.; Liu, J.; Li, Z.; Cao, J.; Liao, S. High Performance Aqueous Zinc-Ion Batteries Developed by PANI Intercalation Strategy and Separator Engineering. *Molecules* **2024**, *29*, 3147. [CrossRef]
44. He, Q.; Bai, J.; Xue, M.; Liao, Y.; Wang, H.; Long, M.; Chen, L. Polypyridine intercalation boosting the kinetics and stability of $\text{V}_3\text{O}_7 \cdot \text{H}_2\text{O}$ cathodes for aqueous zinc-ion batteries. *J. Energy Chem.* **2024**, *97*, 361–370. [CrossRef]
45. Zhang, A.; Yin, X.; Saadoune, I.; Wei, Y.; Wang, Y. Zwitterion Intercalated Manganese Dioxide Nanosheets as High-Performance Cathode Materials for Aqueous Zinc Ion Batteries. *Small* **2024**, *20*, e2402811. [CrossRef] [PubMed]
46. Guo, C.; Yi, S.; Si, R.; Xi, B.; An, X.; Liu, J.; Li, J.; Xiong, S. Advances on Defect Engineering of Vanadium-Based Compounds for High-Energy Aqueous Zinc-Ion Batteries. *Adv. Energy Mater.* **2022**, *12*, 2202039. [CrossRef]
47. Huang, J.; Cao, Y.; Cao, M.; Zhong, J. Improving the capacity of zinc-ion batteries through composite defect engineering. *RSC Adv.* **2021**, *11*, 34079–34085. [CrossRef] [PubMed]
48. Zhang, J.; Liu, R.; Huang, C.; Dong, C.; Xu, L.; Yuan, L.; Lu, S.; Wang, L.; Zhang, L.; Chen, L. Oxygen defect engineering and amphiphatic molecules intercalation co-boosting fast kinetics and stable structure of S-doped $(\text{NH}_4)_2\text{V}_{10}\text{O}_{25} \cdot 8\text{H}_2\text{O}$ free-standing cathode for aqueous Zn-ion storage. *Nano Energy* **2024**, *122*, 109301. [CrossRef]
49. Xiong, T.; Yu, Z.G.; Wu, H.; Du, Y.; Xie, Q.; Chen, J.; Zhang, Y.W.; Pennycook, S.J.; Lee, W.S.V.; Xue, J. Defect Engineering of Oxygen-Deficient Manganese Oxide to Achieve High-Performing Aqueous Zinc Ion Battery. *Adv. Energy Mater.* **2019**, *9*, 1803815. [CrossRef]
50. Bassyouni, Z.; Allagui, A.; Abou Ziki, J.D. Microsized Electrochemical Energy Storage Devices and Their Fabrication Techniques For Portable Applications. *Adv. Mater. Technol.* **2022**, *8*, 2200459. [CrossRef]
51. Shi, X.; Das, P.; Wu, Z.-S. Digital Microscale Electrochemical Energy Storage Devices for a Fully Connected and Intelligent World. *ACS Energy Lett.* **2021**, *7*, 267–281. [CrossRef]
52. Sha, M.; Zhao, H.; Lei, Y. Updated Insights into 3D Architecture Electrodes for Micropower Sources. *Adv. Mater.* **2021**, *33*, e2103304. [CrossRef] [PubMed]
53. Zhu, Z.; Kan, R.; Hu, S.; He, L.; Hong, X.; Tang, H.; Luo, W. Recent Advances in High-Performance Microbatteries: Construction, Application, and Perspective. *Small* **2020**, *16*, e2003251. [CrossRef]
54. Naresh, N.; Zhu, Y.; Luo, J.; Fan, Y.; Wang, T.; Raju, K.; De Volder, M.; Parkin, I.P.; Boruah, B.D. Advanced 3D Micro-Electrodes for On-Chip Zinc-Ion Micro-Batteries. *Adv. Funct. Mater.* **2024**, *35*, 2413777. [CrossRef]
55. Liu, G.; Ma, Z.; Li, G.; Yu, W.; Wang, P.; Meng, C.; Guo, S. All-Printed 3D Solid-State Rechargeable Zinc-Air Microbatteries. *ACS Appl. Mater. Interfaces* **2023**, *15*, 13073–13085. [CrossRef]
56. Yao, B.; Chandrasekaran, S.; Zhang, J.; Xiao, W.; Qian, F.; Zhu, C.; Duoss, E.B.; Spadaccini, C.M.; Worsley, M.A.; Li, Y. Efficient 3D Printed Pseudocapacitive Electrodes with Ultrahigh MnO_2 Loading. *Joule* **2019**, *3*, 459–470. [CrossRef]
57. Huang, H.; Liao, L.; Lin, Z.; Pan, D.; Nuo, Q.; Wu, T.T.; Jiang, Y.; Bai, H. Direct Ink Writing of Pickering Emulsions Generates Ultralight Conducting Polymer Foams with Hierarchical Structure and Multifunctionality. *Small* **2023**, *19*, 2301493. [CrossRef] [PubMed]
58. Zhou, S.; Li, M.; Wang, P.; Cheng, L.; Chen, L.; Huang, Y.; Yu, S.; Mo, F.; Wei, J. Printed Solid-State Batteries. *Electrochem. Energy Rev.* **2023**, *6*, 34. [CrossRef]
59. Lu, Y.; Wang, Z.; Li, M.; Li, Z.; Hu, X.; Xu, Q.; Wang, Y.; Liu, H.; Wang, Y. 3D Printed Flexible Zinc Ion Micro-Batteries with High Areal Capacity Toward Practical Application. *Adv. Funct. Mater.* **2023**, *34*, 2310966. [CrossRef]
60. Wang, X.; Zheng, S.; Zhou, F.; Qin, J.; Shi, X.; Wang, S.; Sun, C.; Bao, X.; Wu, Z.S. Scalable fabrication of printed Zn/MnO_2 planar micro-batteries with high volumetric energy density and exceptional safety. *Natl. Sci. Rev.* **2020**, *7*, 64–72. [CrossRef] [PubMed]
61. Cai, X.; Liu, Y.; Zha, J.; Tan, F.; Zhang, B.; Yan, W.; Zhao, J.; Lu, B.; Zhou, J.; Tan, C. A Flexible and Safe Planar Zinc-Ion Micro-Battery with Ultrahigh Energy Density Enabled by Interfacial Engineering for Wearable Sensing Systems. *Adv. Funct. Mater.* **2023**, *33*, 2303009. [CrossRef]
62. Zhao, J.; Lu, H.; Zhang, Y.; Yu, S.; Malyi, O.I.; Zhao, X.; Wang, L.; Wang, H.; Peng, J.; Li, X.; et al. Direct coherent multi-ink printing of fabric supercapacitors. *Sci. Adv.* **2021**, *7*, eabd6978. [CrossRef] [PubMed]
63. Li, X.; Jin, X.; Wang, Y.; Zhang, X.; Li, D.; Wang, J.; Yuan, M.; Liu, J.; Zhao, Y. All-Direct Laser Patterning Zinc-Based Microbatteries. *Adv. Funct. Mater.* **2023**, *34*, 2314060. [CrossRef]

64. Shi, X.; Wu, Z.S.; Qin, J.; Zheng, S.; Wang, S.; Zhou, F.; Sun, C.; Bao, X. Graphene-Based Linear Tandem Micro-Supercapacitors with Metal-Free Current Collectors and High-Voltage Output. *Adv. Mater.* **2017**, *29*, 1703034. [CrossRef] [PubMed]
65. Lan, X.; Tang, T.; Xie, H.; Hasan, S.W.; Liang, L.; Tian, Z.Q.; Shen, P.K. Robust, Conductive, and High Loading Fiber-Shaped Electrodes Fabricated by 3D Active Coating for Flexible Energy Storage Devices. *Nano Lett.* **2022**, *22*, 5795–5802. [CrossRef]
66. Zhao, J.; Ma, Z.; Qiao, C.; Fan, Y.; Qin, X.; Shao, G. Spectroscopic Monitoring of the Electrode Process of MnO_2 @rGO Nanospheres and Its Application in High-Performance Flexible Micro-Supercapacitors. *ACS Appl. Mater. Interfaces* **2022**, *14*, 34686–34696. [CrossRef] [PubMed]
67. Liu, H.; Zhang, G.; Wang, L.; Zhang, X.; Zhao, Z.; Chen, F.; Song, L.; Duan, H. Engineering 3D Architecture Electrodes for High-Rate Aqueous Zn-Mn Microbatteries. *ACS Appl. Energy Mater.* **2021**, *4*, 10414–10422. [CrossRef]
68. Li, R.; Li, L.; Jia, R.; Jiang, K.; Shen, G.; Chen, D. A Flexible Concentric Circle Structured Zinc-Ion Micro-Battery with Electrode-deposited Electrodes. *Small Methods* **2020**, *4*, 2000363. [CrossRef]
69. Wang, G.-Y.; Li, G.-X.; Tang, Y.-D.; Zhao, Z.; Yu, W.; Meng, C.-Z.; Guo, S.-J. Flexible and Antifreezing Fiber-Shaped Solid-State Zinc-Ion Batteries with an Integrated Bonding Structure. *J. Phys. Chem. Lett.* **2023**, *14*, 3512–3520. [CrossRef]
70. Wang, X.; Wu, Z.S. Zinc based micro-electrochemical energy storage devices: Present status and future perspective. *EcoMat* **2020**, *2*, e12042. [CrossRef]
71. Gao, T.; Yan, G.; Yang, X.; Yan, Q.; Tian, Y.; Song, J.; Li, F.; Wang, X.; Yu, J.; Li, Y.; et al. Wet spinning of fiber-shaped flexible Zn-ion batteries toward wearable energy storage. *J. Energy Chem.* **2022**, *71*, 192–200. [CrossRef]
72. Xia, Z.; Li, S.; Wu, G.; Shao, Y.; Yang, D.; Luo, J.; Jiao, Z.; Sun, J.; Shao, Y. Manipulating Hierarchical Orientation of Wet-Spun Hybrid Fibers via Rheological Engineering for Zn-Ion Fiber Batteries. *Adv. Mater.* **2022**, *34*, 2203905. [CrossRef]
73. Zhang, H.; Xiong, T.; Zhou, T.; Zhang, X.; Wang, Y.; Zhou, X.; Wei, L. Advanced Fiber-Shaped Aqueous Zn Ion Battery Integrated with Strain Sensor. *ACS Appl. Mater. Interfaces* **2022**, *14*, 41045–41052. [CrossRef] [PubMed]
74. Li, T.; Xu, Q.; Waqar, M.; Yang, H.; Gong, W.; Yang, J.; Zhong, J.; Liu, Z. Millisecond-induced defect chemistry realizes high-rate fiber-shaped zinc-ion battery as a magnetically soft robot. *Energy Storage Mater.* **2023**, *55*, 64–72. [CrossRef]
75. Li, Y.; Guan, Q.; Cheng, J.; Wang, B. Amorphous $\text{H}_{0.82}\text{MoO}_{3.26}$ cathodes based long cyclife fiber-shaped Zn-ion battery for wearable sensors. *Energy Storage Mater.* **2022**, *49*, 227–235. [CrossRef]
76. Ho, C.C.; Evans, J.W.; Wright, P.K. Direct write dispenser printing of a zinc microbattery with an ionic liquid gel electrolyte. *J. Micromech. Microeng.* **2010**, *20*, 104009. [CrossRef]
77. Zeng, Y.; Zhang, X.; Meng, Y.; Yu, M.; Yi, J.; Wu, Y.; Lu, X.; Tong, Y. Achieving Ultrahigh Energy Density and Long Durability in a Flexible Rechargeable Quasi-Solid-State Zn-MnO₂ Battery. *Adv. Mater.* **2017**, *29*, 1700274. [CrossRef]
78. Zheng, Z.; Cheng, W.; Jiang, G.; Li, X.; Sun, J.; Zhu, Y.; Zhao, D.; Yu, H. Ethanol Vapor-Induced Synthesis of Robust, High-Efficiency Zinc Ion Gel Electrolytes for Flexible Zn-Ion Batteries. *Small Struct.* **2024**, *5*, 2400180. [CrossRef]
79. Jin, X.; Song, L.; Dai, C.; Ma, H.; Xiao, Y.; Zhang, X.; Han, Y.; Li, X.; Zhang, J.; Zhao, Y.; et al. A self-healing zinc ion battery under -20°C . *Energy Storage Mater.* **2022**, *44*, 517–526. [CrossRef]
80. Shi, J.; Wang, S.; Chen, X.; Chen, Z.; Du, X.; Ni, T.; Wang, Q.; Ruan, L.; Zeng, W.; Huang, Z. An Ultrahigh Energy Density Quasi-Solid-State Zinc Ion Microbattery with Excellent Flexibility and Thermostability. *Adv. Energy Mater.* **2019**, *9*, 1901957. [CrossRef]
81. Wang, X.; Li, Y.; Wang, S.; Zhou, F.; Das, P.; Sun, C.; Zheng, S.; Wu, Z.S. 2D Amorphous V₂O₅/Graphene Heterostructures for High-Safety Aqueous Zn-Ion Batteries with Unprecedented Capacity and Ultrahigh Rate Capability. *Adv. Energy Mater.* **2020**, *10*, 2000081. [CrossRef]
82. Zhang, X.; Hu, L.; Zhou, K.; Zhang, L.; Zeng, X.; Shi, Y.; Cai, W.; Wu, J.; Lin, Y. Fully Printed and Sweat-Activated Micro-Batteries with Lattice-Match Zn/MoS₂ Anode for Long-Duration Wearables. *Adv. Mater.* **2024**, *36*, e2412844. [CrossRef] [PubMed]
83. Lee, S.H.; Hwang, J.; Song, C.; Park, C.; Kim, H.S.; Ahn, H. Zinc-Ion Microbatteries with High Operando Dynamic Stretchability Designed to Operate in Extreme Environments. *Adv. Funct. Mater.* **2023**, *34*, 2310571. [CrossRef]
84. Shi, S.; Zhou, D.; Jiang, Y.; Cheng, F.; Sun, J.; Guo, Q.; Luo, Y.; Chen, Y.; Liu, W. Lightweight Zn-Philic 3D-Cu Scaffold for Customizable Zinc Ion Batteries. *Adv. Funct. Mater.* **2024**, *34*, 2312664. [CrossRef]
85. Meng, F.; Ren, Y.; Ping, B.; Huang, J.; Li, P.; Chen, X.; Wang, N.; Li, H.; Zhang, L.; Zhang, S.; et al. Five-Axis Curved-Surface Multi-Material Printing on Conformal Surface to Construct Aqueous Zinc-Ion Battery Modules. *Adv. Mater.* **2024**, *36*, e2408475. [CrossRef]

Disclaimer/Publisher’s Note: The statements, opinions and data contained in all publications are solely those of the individual author(s) and contributor(s) and not of MDPI and/or the editor(s). MDPI and/or the editor(s) disclaim responsibility for any injury to people or property resulting from any ideas, methods, instructions or products referred to in the content.